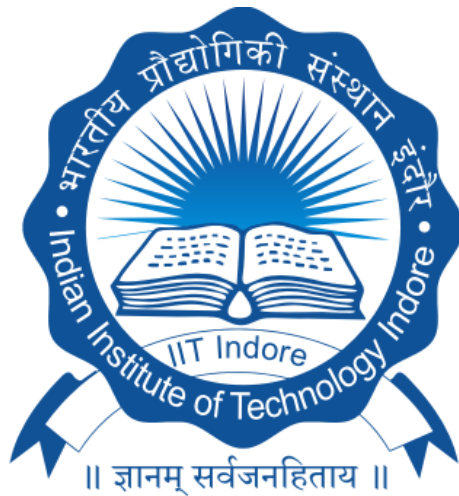


ASSESSMENT OF PARKER SOLAR PROBE DATA USING SWASTI-SW FRAMEWORK

M.Sc. Thesis

By:
Sumit Gautam



**DEPARTMENT OF ASTRONOMY , ASTROPHYSICS AND
SPACE ENGINEERING**

**INDIAN INSTITUTE OF TECHNOLOGY
INDORE**

April, 2023

ASSESSMENT OF PARKER SOLAR PROBE DATA USING SWASTI-SW FRAMEWORK

A THESIS

*Submitted in partial fulfillment of the
requirements for the award of the degree
of
Master of Science*

by
Sumit Gautam



**DEPARTMENT OF ASTRONOMY , ASTROPHYSICS AND
SPACE ENGINEERING**

**INDIAN INSTITUTE OF TECHNOLOGY
INDORE**

April, 2023

INDIAN INSTITUTE OF TECHNOLOGY INDORE

CANDIDATE'S DECLARATION

I hereby certify that the work which is being presented in the thesis entitled "**Assessment of Parker Solar Probe data using SWASTi-SW Framework**" in the partial fulfillment of the requirements for the award of the degree of MASTER OF SCIENCE and submitted in the DEPARTMENT OF ASTRONOMY , ASTROPHYSICS AND SPACE ENGINEERING , Indian Institute of Technology Indore, is an authentic record of my own work carried out during the time period from July, 2022 to May, 2023 under the supervision of Dr. Bhargav Vaidya . The matter presented in this thesis has not been submitted by me for the award of any other degree of this or any other institute.

**Signature with date
(Sumit Gautam)**

This is to certify that the above statement made by the candidate is correct to the best of my knowledge.

Signature of the Supervisor of
M.Sc. Thesis
(DR. BHARGAV VAIDYA)

Sumit Gautam has successfully given his M.Sc. Oral Examination held on

Signature(s) of Supervisor(s) of
MSc thesis, Date:

Convener, DPGC
Date:-

Signature of PSPC Member 1
Date:-

Signature of PSPC Member 2
Date:-

Signature of PSPC Member 3
Date:-

ABSTRACT

Solar wind streams have a significant impact on the propagation of space weather drivers within the heliosphere, ultimately resulting in geomagnetic storm activity. This serves as important contextual information. The heart of space weather forecasting lies in the anticipation of solar wind properties. The Parker Solar Probe (PSP) was launched by NASA in August 2018 with the aim of investigating the inner heliosphere. The mission seeks to provide insights into the solar corona's heating, the acceleration and source of the solar wind, as well as solar energetic particles. Numerous unanswered questions in these areas are expected to be addressed through the PSP mission. The Parker Solar Probe (PSP) represents the pioneering in-situ investigation of the solar corona, with its nearest perihelion point currently located at a distance of 13.3 solar radii from the Sun, as of June 9, 2022. According to estimates, the spacecraft will reach below 10R on its 22nd orbit in mid 2024. The objective of this investigation is to conduct a comparative analysis between the in-situ solar wind observation of the Parker Solar Probe (PSP) in the inner heliosphere and the solar wind simulation outcomes of the Solar Wind from SWASTi-SW model. The purpose of this comparison is to evaluate the reliability and validity of the SWASTi-SW model in relation to the in-situ data. SWASTi-SW is a data-driven three-dimensional physics-based solar wind model. It is based on a two-domain approach, which includes a semi-empirical coronal domain and an inner heliospheric domain based on MHD. We provide our model's forecast for the first and second perihelion of PSP, which happened in November 2018 and March 2019, respectively. New information on solar wind acceleration is revealed by contrasting the MHD results with the PSP measurements. The accuracy of the Air Force Data Assimilative Photospheric flux Transport-based estimations is further demonstrated by PSP measurements across the inner heliosphere. We found that SWASTi model works better for in-situ data with the adapt input magnetogram. Comparison of the SWASTi-SW outputs with Parker Solar Probe in-situ observation can provide new understanding of solar wind acceleration.

Contents

1	Introduction	1
1.1	Space Weather	1
1.2	Space weather events	1
1.2.1	CME (Coronal Mass Ejection)	1
1.2.2	Solar Flares	2
1.2.3	Solar Wind	2
1.3	Importance of Space weather and It's forecasting	3
1.4	Missions to Study Space Weather/SUN	5
1.4.1	Parker Solar Probe	9
1.5	Space Weather Forecasting Models	15
1.6	Motivation	16
2	Theoretical Aspect	17
2.1	Parker's Solar Wind	17
2.2	Stellar winds	19
2.3	Coordinate System	19
2.3.1	Spacecraft Coordinate System	20
2.3.2	Coordinate conversion	21
2.3.3	Magnetogram	22
2.4	MHD Model:- Space Weather Adaptive Simulation Framework for Solar Wind (SWASTi-SW)	25
2.4.1	Comparing SWASTi-SW model Data from Omni Data at 1 AU(Past study)	27
3	Methodology	29
3.1	Data Products (PSP)	30
3.2	Data collection	31
4	Results	32
4.1	Results:CR2210	32
4.1.1	Using Gong Magnetogram	32
4.1.2	Using Adapt Synoptic Maps	35
4.1.3	Perihelion 2 of PSP (CR2215 and CR2216)	41
5	Conclusion and Future Goals	45
6	Data Availability	47

REFERENCES

List of Figures

1.1	Coronal Mass Ejection	2
1.2	Solar Flare	3
1.3	Geomagnetic Strom event on March 13,1989	4
1.4	Parker Solar Probe Instrument	10
1.5	SWEAP device	11
1.6	SWEAP suits four sensors	12
1.7	Parker Solar Probe Trajectory	14
2.1	Parker's solar wind (1)	18
2.2	Parker Spiral	18
2.3	Adapt Working	24
2.4	Flow diagram of SWASTi-SW	26
2.5	Comparision of model and omini data(past study)	28
4.1	PSP and Model comparision (CR2210)	33
4.2	Omini and model comparision (CR2210)	34
4.3	Input and source surface magnetic field of Adapt	35
4.4	Snapshot of model	36
4.5	PSP and Model comparision (CR2210) From Adpat Input	37
4.6	Omini and model comparision (CR2210)	38
4.7	Radial components of velocity profile of model at 1AU with different inputs	38
4.8	Radial components of velocity profile of HUX and MHD with observed data at 1AU (Input Adapt)	39
4.9	MHD comparison with NASA's Enlil (CR2210)	40
4.10	Input and source surface magnetic field of Adapt	41
4.11	Snapshot of model	42
4.12	PSP and Model comparison (CR2215 and CR2216) From Adpat Input	43
4.13	Omni and Model comparison (CR2215) From Adpat Input	44

Chapter 1

Introduction

1.1 Space Weather

Space Weather is a very vast and important subject to study nowadays. Space weather is defined as the dynamic circumstances on the Sun and in the Sun-Earth medium that can have a significant impact on the operation of space-borne and ground-based technological equipment, consequently influencing human existence. The Sun is the main source of energy on Earth, and space weather events are any occurrences that are caused by changes in the Solar atmosphere and affect the Sun-Earth relationship. These Space Weather events have a direct influence on our life and must be handled as seriously as our typical weather activities.

1.2 Space weather events

Solar energetics particles, coronal mass ejection, high - speed solar wind, and solar flares are examples of space weather events. These events are governed by the solar magnetic field.

1.2.1 CME (Coronal Mass Ejection)

The corona, or outer part solar atmosphere, is formed by intense magnetic forces. The locations where these magnetic fields are closed, commonly over groups of sunspots (A sunspot is a region on the solar surface with the high magnetic field strengths that show a highly twisted topology), the constrained solar environment can abruptly and magnetic fields and harshly expel bubbles of gas known as coronal mass ejections. A huge CME can include billions of tonnes of materials. which, in a spectacular explosion, can be accelerated to millions of miles per hour. Solar material flows over into the IM (interplanetary medium), crashing onto a spacecraft and space probe in its path. CME are frequently connected with flares, although they can also happen on their own. CMEs are key source of hazardous space weather condition on the Earth.

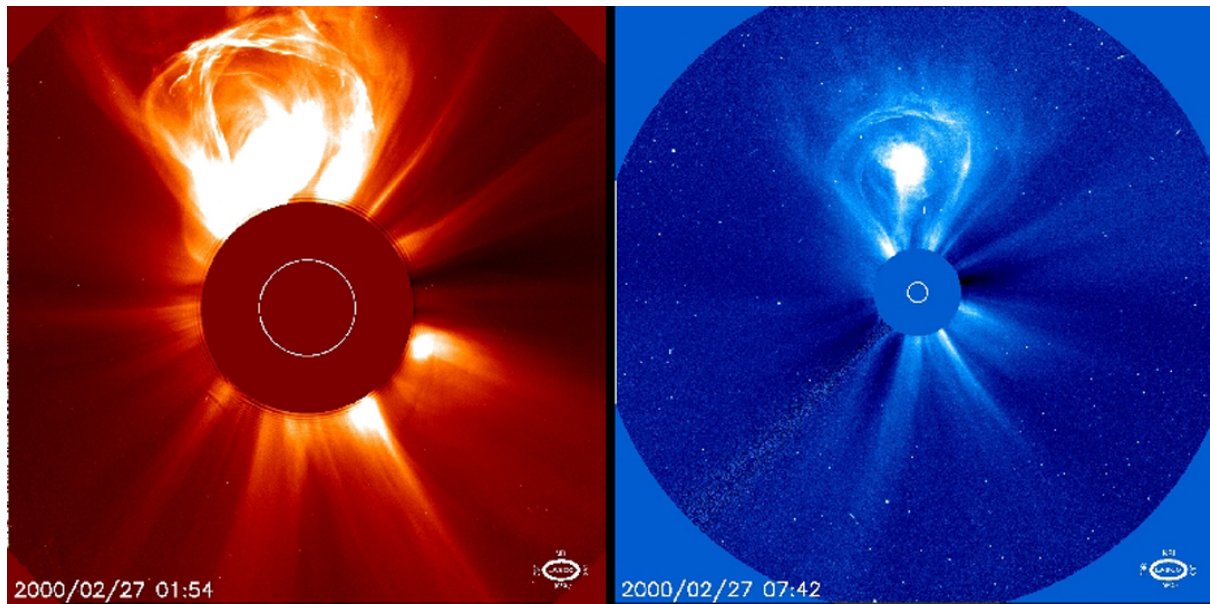


Figure 1.1: CME on 27/02/2000 taken by C3 and SOHO LASCO C2. A CME launches billions of tonnes of particles into space at speeds of millions of miles per hour. Credits: ESANASA/SOHO

1.2.2 Solar Flares

A solar flare is a massive explosion that occurs on the Sun when energy trapped in magnetic fields that are "twisted" (often above sunspots) is abruptly released. It is the solar system's most explosive phenomenon. They are seen as brilliant spots on the sun and might last for a short while or for several hours. The brightness of solar flares in x-ray wavelengths is used by scientists to categorise them. There are three kinds of solar flare: Significant events such as large-scale X-class flares have the ability to trigger both severe global radio blackouts and in the high radiation the radiation storms. Medium-sized M-class flares typically result in short radio collapse that impact polar regions of Earth. Occasionally an M-class flare is followed by small radiation storms. C-class flares are minor and have little effects on Earth when compared to X- and M-class occurrences. X-rays and optical light are the main monitoring tools for flares. Coronal mass ejections (CMEs), which were long believed to be started by solar flares, are distinct from solar flares. Huge gas bubbles that are blasted from the Sun over the period of many hours are called CMEs. They are laced with magnetic field lines. Although some CMEs are accompanied with flares, it is now recognised that the majority of CMEs are not. A high intensity Solar Flare is usually a signal for the advent of catastrophic space weather phenomena.

1.2.3 Solar Wind

Eugene Newman Parker initially deduced that the By pressure balance, the solar corona can not be in hydrostatic equilibrium and so must be spreading outwards, resulting in the concept of a dynamic outflow of plasma filling up the whole interplanetary domain. This is known as solar wind. The solar wind is mainly made up of electrons and protons, with a few heavier ions mixed.

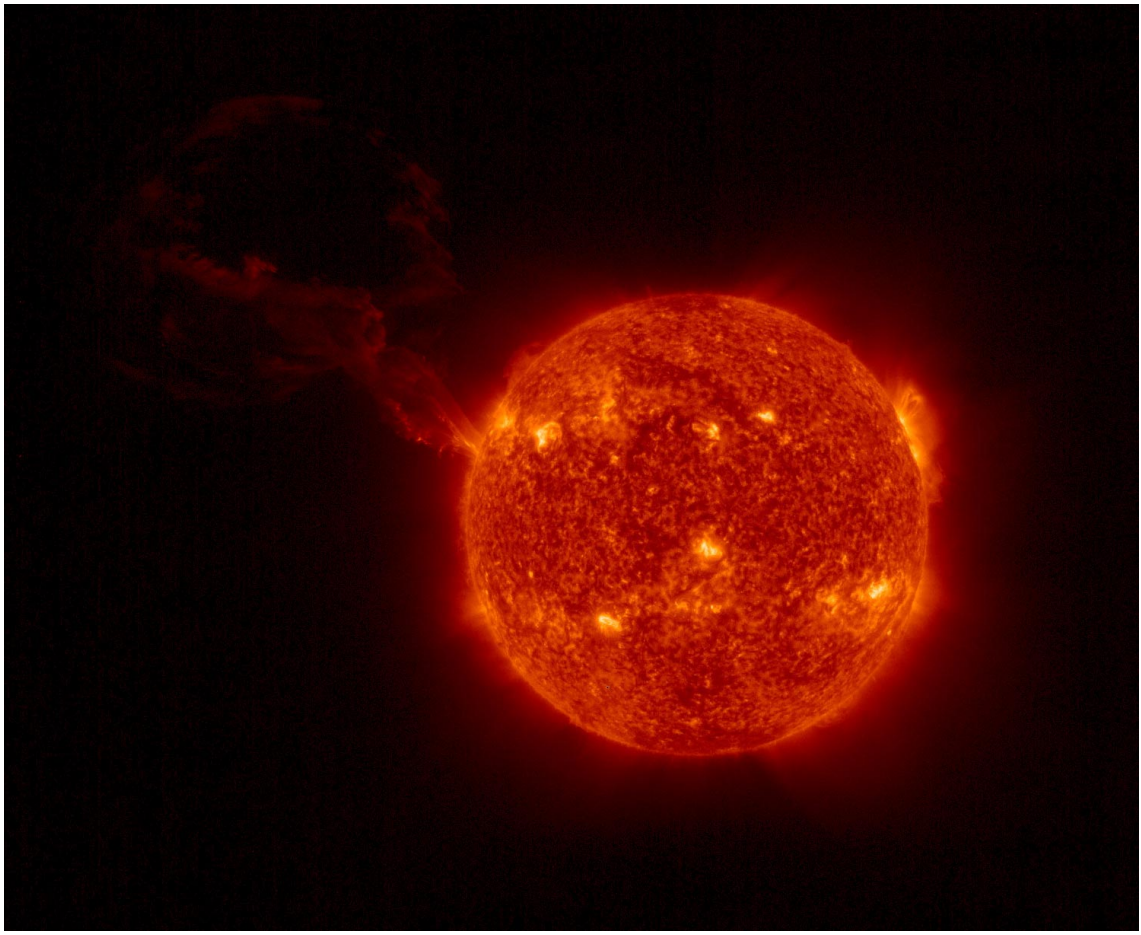


Figure 1.2: On 15/02/2022, a massive solar eruption was photographed by the Full Sun Imager of the High Uv Imaging device on board the ESA/NASA Solar Orbiter mission.

As a background, solar wind streams influence the spread of space weather drivers in the heliosphere, which cause geomagnetic storm activity. As a result, space weather forecasts are based on the prediction of solar wind characteristics.

1.3 Importance of Space weather and It's forecasting

As we said in the preceding section, space weather is principally caused by the Sun, It continuously transmits energy and particles to Earth through the solar wind. However, We are shielded from hazardous space weather activities by the Earth's magnetic field. In the absence of the magnetosphere, the solar wind could rip apart earth's atmosphere. A space weather event that was among the most severe in modern times struck the planet twenty years ago. As we all know, modern society is dependent on a wide range of devices that are vulnerable to space weather extremes. Over the Earth's surface powerful electrical currents generated during the auroral outbursts suspend power grids and lead to pipeline corrosion. Geomagnetic storms affect the ionosphere, which affects GPS navigation and high-frequency radio transmissions. Radio communications for commercial airliners flying transpolar routes can be disrupted during events of polar cap absorption triggered by protons. When solar energetic particle events and radiation belt increases occur, spacecraft exposure to energetic particles causes temporary operational issues,

harm to critical electronics, damage of solar arrays, and blinding of optical systems like imagers and star trackers.

A CME the size of 36 Earths once erupted from the sun's turbulent surface on March 10, 1989, and it traveled through space at a million miles per hour (1.6 million kilometres per hour). Two days later, the powerful solar jetsam and solar wind were deflected by the torrid gas cloud colliding with Earth's magnetosphere. The geomagnetic superstorm was sparked by this solar flare's dramatic disruption of the magnetosphere.

As a result, stakeholders in government and industry as well as the scientific community appreciate the value of space weather forecasting. ([Schrijver et al., 2015](#)).

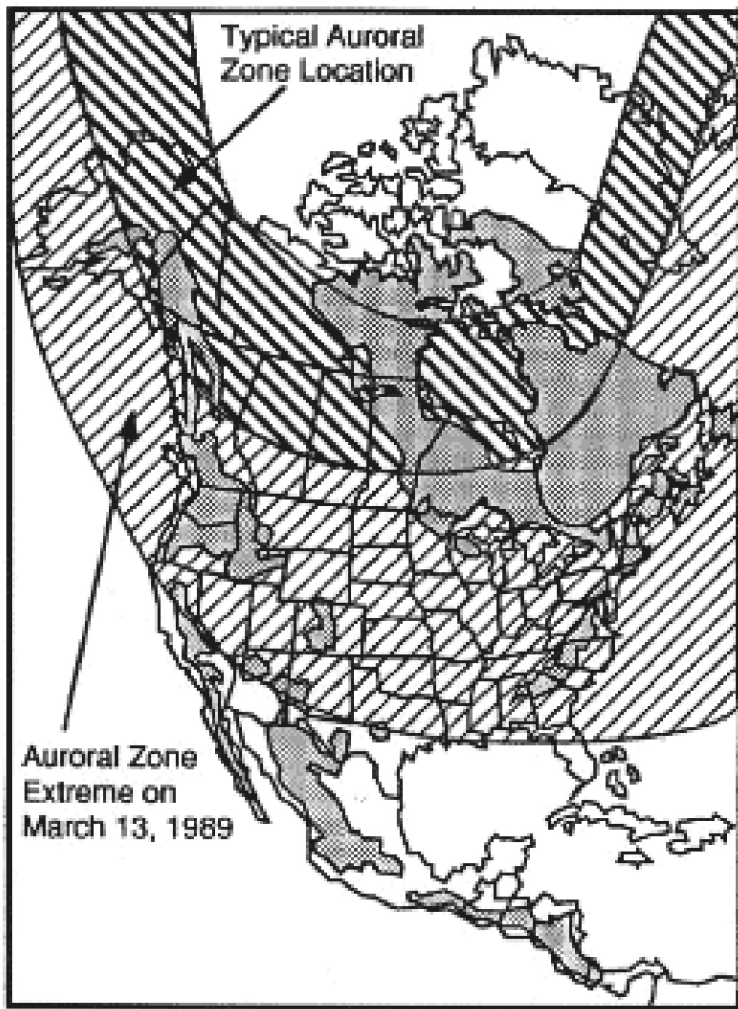


Figure 1.3: The impacts of high geomagnetic activity are especially dangerous to power systems in places with igneous rock (grey) because the power transmission lines located above the igneous rock are encouraged to conduct geomagnetically induced currents (GICs) by the high resistance of the granite. The auroral zone and the extremes that the aurora may reach during powerful disturbances like the one on March 13, 1989, are displayed in cross-hatching. Credits: American Geophysical Union

Solar activity affects both human and robotic explorers throughout the solar system. Space weather events can disrupt surface-to-orbit and surface-to-surface communications.

1.4 Missions to Study Space Weather/SUN

As we discussed above that how important is the study of space weather and behaviour of Sun , So its also important to understand these things . Nasa and other space agencies frequently keep sending missions to study Sun. Various Space mission to for the study of Sun are following:-

Ulyssess(1990)

Nasa and ESA sent the Ulyssess in 1990 , which is first mission by human kind for the study of Sun. This probe operated more than four times its expected lifetime and made many important discoveries.

Yohkoh(1991)

On August 30, 1991, the US, the UK, and Japan's Institute of Space and Astronautical Sciences launched the Yohkoh mission. Yoh-koh, which means 'sunbeam' in Japanese, four instruments were carried by it to study and understand the Sun in hard and soft x-rays, as well as at energies of gamma ray. Yohkoh's soft x-ray telescope was created by engineers and scientists of the ATC's Solar Astrophysics Laboratory (SXT). Over the course of its 10 years and 4 months of solar investigations, Yohkoh made a number of significant findings regarding the solar flares , space weather and solar corona. The roughly 11-year cycle in which the Sun changes from a period of relative calm to a period of numerous severe storms and sunspots, and then back again, was the first time a spacecraft has continually observed the Sun in x-rays.

Wind(1994)

On 01/11/1994, NASA launched Wind, a spin-stabilized spacecraft, using a Delta II rocket. Early in 2004, after multiple orbits through the magnetosphere, Wind was launched into a Lissajous orbit at L1 Lagrange point, more than two hundred Re upstream of Earth, to track the unaffected solar wind approaching Earth's magnetosphere. After some time Wind was placed in halo orbit at L1(2020).

SOHO(1995)

NASA and SOHO collaborative project of Solar and Heliospheric Observatory (SOHO) was created to understand the Sun from the inside out, from its internal structure to its vast outer atmosphere to the solar wind that it blasts throughout the solar system. SOHO was supposed to run until 1998 when it was launched in December 1995, but because it has been so successful, ESA and NASA have approved a number of mission extensions over the past 20 years, enabling it to cover numerous solar cycles (Eleven year periods of solar activity). Over the last 20 years, SOHO has produced a number of significant discoveries in space that have enhanced astronomers' knowledge of our closest star. First images of the convective zone on the Sun have been taken by SOHO, or turbulent top

layer of its centre, moreover the structure of sunspots under the solar surface. It has also produced extensive measurements of the interior as well as slow and fast solar wind, as well as pinpointing source locations and acceleration processes. Over Along with new dynamic solar phenomena like coronal waves and solar storms, over 3,000 new comets have been discovered. 12 instruments created by 29 universities across 15 countries are provided at SOHO. The numerous equipment enable SOHO to undertake a wide variety of science, from collecting photographs of the Sun and surrounding atmosphere to studying particular wavelengths and the makeup of that light to monitoring energetic particles passing by the spacecraft.

ACE(1997)

NASA designed and launched the Advanced Composition Explorer (ACE) mission to study energetic interplanetary particles coming from the Sun-Earth Lagrange point 1 , which is approximately 870k miles (about 1.4 MKm) from Earth. It launched at 25 Aug ,1997 and on 21 jan 1998 the spacecraft begun operations. In order to determine the similarities and interactions between the Earth, Sun and the Milky Way galaxy, a spacecraft was launched primarily to study the solar material. Additionally, ACE provides enhanced geomagnetic storm warnings and real-time space weather data. The gathering power of ACE's nine instruments is 10 to 10,000 times higher than anything in past flown. The spaceship has lasted significantly longer than predicted.

TRACE(1998)

NASA launched the Transition Region and Coronal Explorer (TRACE) on April 1, 1998. This was the first mission to photograph the whole solar cycle. observing the sun at both its turbulent maximum and its calm lowest. It was a satellite mission aimed to investigate the relationships between the corresponding grand-scale plasma structures and fine-scale magnetic fields on the sun in order to aquire a greater understanding of our dynamic solar's activity. TRACE captured images of the magnetic structures that arise from the photosphere - the sun's evident surface - and eventually shape the dynamics and geometry of the upper atmosphere of Sun, which is made up of the transition area and corona.

CLUSTER(2000)

Cluster is a group of four spacecraft travelling in formation around the Earth. They provide the most precise information on how the solar wind impacts our world in three dimensions ever. Solar wind (the Sun's constant stream of subatomic particles) can harm communications satellites and power plants on Earth. The Cluster mission's intended operational life span was from February 2001 to January 2003. The mission is still going strong twenty years after it was launched.

RHESSI(2002)

A NASA SMEX (Small Explorer) solar mission called Reuven Ramaty High Energy Solar Spectroscopic Imager (RHESSI) was launched in February 2002 and is operated for NASA/GSFC by the Berkeley's Space Science Laboratory (SSL) (UCB) University of California. The ultimate goal was to investigate the energy release in solar flares and fundamental physics of particle acceleration. With high resolution spanning from 3 keV X-rays - 17 MeV GR(gamma rays); simultaneous, spectroscopy of solar flares and high resolution imaging are the main observations. RHESSI (originally - HESSI) is a partnership of PSI (Paul Scherrer Institut, Villigen, Switzerland),UCB (PI: Robert P. Lin), GSFC and ETH Zürich (HESSI Experimental Data Center - HEDC).

Double Star(2003)

To better understand how the Sun affects the Earth's environment, particularly the "magnetic tail" where storms of high-energy particles occur, the ESA and Chinese governments collaborated on the Double Star project. By exploring the impact of the Sun on the Earth's ecosystem, Double Star was a follow-up to the revolutionary Cluster project from the European Space Agency. It looked into the magnetosphere, or the magnetic bubble that surrounds our planet. As the name implies, Double Star featured two spacecraft flying in complimentary orbits around the Earth, each planned, launched, constructed, and controlled by the Space Administration of China National. One Double Star spacecraft was in polar orbit, while the other was near the equator. This structure allowed scientists to simultaneously gather information on the number of electrified particles and the changing magnetic field in several magnetosphere sites. In December 2003 and July 2004, the pair was launched from two distinct launch locations in China. This timetable allowed them to work alongside ESA's Cluster project. It consists of four similar spaceprobe launched into elliptical orbits surrounding Earth as a mini flotilla. On October 14, 2007, satellite TC-1 was deactivated and burnt up as it re-entered the atmosphere of Earth, bringing an end to the Double Star mission.

Stereo(2006)

The Solar Terrestrial Relations Observatory, or STEREO, was went to space in 2006 October and has contribute to scientists with a unique and groundbreaking picture of the Earth Sun System. STEREO has traced the motion of energy and matter from the Sun to Earth by using two almost similar observatories, one ahead of Earth in its orbit and the other following behind.

HINODE(2006)

Hinode is a multinational project to investigate the Sun, our closest star. Hinode investigates the amgnetic fields of Sun's for the sake of a better understanding of what fuels the atmosphere of Sun and drives solar eruptions. The Solar Optical Telescope from Hinode is the 1st space probe device to get the intensity and direction of the magnetic field of Sun on the photosphere. Hinode travels around Earth in a Sun-synchronous orbit at a

height of roughly 400 miles (a little under 650 km). Due to Hinode's orbit, it can observe the Sun nonstop for nine months. In each 98-minute orbit of Hinode, the Sun is obscured by Earth for up to 10 minutes during the summertime (in the northern hemisphere).

Proba-2(2009)

Full name of PROBA project is The PRoject for OnBoard Autonomy (PROBA). This missions is a set of many microsatellites , which launched by the (ESA)European Space Agency to serve as a testing platform for innovative technologies in orbit. The 2nd satellite in the program, PROBA2, was sent into orbit on 2/11/2009. PROBA2's major mission purpose is to conduct an in-flight demonstration of a number of novel space probes technologies. The secondary mission purpose is to use the payload of instruments, this consists of the Large Yield Radiometer, Image Processing, the Sun Watcher with Active Pixel Sensor, and two sun-sensing equipment. Both sensors are technologically distinctive, but they also contribute unique scientific data to the solar physics community.

Solar Dynamics Observatory(2010)

NASA's Solar Dynamics Observatory, or SDO, was launched in 2010 to study how the Sun generates solar activity and causes space weather – the dynamic conditions in space that affect the whole solar system, including Earth. Our knowledge of our closest star, including its interior, atmosphere, magnetic field, and method of energy generation, has greatly benefited from the observations of the Sun made by SDO. The solar dynamo, which is the internal churning that creates the magnetic field that produces space weather, is where SDO measurements start in the Sun's interior. SDO also monitors the solar surface to directly measure the the solar atmosphere and magnetic field in order to understand how magnetic energy is related to the interior and transformed to space weather-causing events.

IRIS(2013)

IRIS, a NASA Small Explorer Mission, was created to investigate the motion, energy absorption, and heating of solar material as it passes through a little explored zone of the Sun's lower atmosphere. From the Californian Vandenberg Air Force Base, IRIS launched out on June 27, 2013.

Solar Orbiter(2020)

Newly launched Solar Orbiter will study the Sun in cooperation with the European Space Agency and NASA. It launched at 11:03 p.m. EST Sunday on a United Launch Alliance Atlas V rocket. It presently orbits the Sun in an elliptical orbit, completing one revolution every 168 days. Solar Orbiter is progressively raising itself off of the ecliptic plane, eventually arriving an angle of 24° above the Sun's equator, thanks to gravity aids from Venus and Earth. Solar Orbiter is obtaining the first photographs of the Sun's south and north poles from high latitudes from this vantage point. Solar Orbiter can almost catch up to the Sun's rate of rotation at its quickest, allowing the spacecraft to hover above

particular places on the Sun as it rotates and examine how a single solar feature changes over time.

ADITYA-L1

The first observatory class space type solar mission from India is called Aditya-L1. The initial Lagrange point, or L1, of the Sun-Earth system will serve as the spacecraft's home base. The main benefit of a satellite orbiting the L1 point is that it can continually see the Sun without being obscured by clouds or eclipses. The advantage of regularly watching solar activity is greater from this position. Aditya-L1 is equipped with seven payloads that use particle and electromagnetic detectors to study the photosphere, chromosphere, and the Sun's outermost layers (the corona). The last 3 payloads conduct in-situ investigations of fields and particles at the Lagrange point L1, while the remaining four payloads observe the Sun directly from the exceptional vantage point of L1. Aditya-L1 will be launched by PSLV-XL from one of the ISRO sites at Sriharikota in the first quarter of 2023. The satellite's scientific investigations will improve our understanding of the Solar Corona and give crucial information for studies of space weather.

1.4.1 Parker Solar Probe

In 2018, the Parker Solar Probe was launched under the auspices of the Johns Hopkins University Applied Physics Laboratory (APL), which is responsible for the program's management on behalf of NASA. The probe was created and is currently being operated by APL. The probe is venturing closer to the Sun than any previous mission in order to investigate the mechanisms responsible for propelling and transporting the solar wind and energetic particles throughout our solar system. In April 2021, Parker achieved a historic milestone by penetrating the solar atmosphere, thereby accessing one of the few unexplored regions of the solar system. The PSP, or Parker Solar Probe, is a spacecraft that is primarily oriented towards the Sun and stabilized along three axes. It follows an elliptical heliocentric orbit with its farthest point, or aphelion, located between the orbits of Venus and Earth. The PSP mission employed multiple Venus gravity assists from August 2018 to March 2025 to gradually decrease the perihelion distance of the spacecraft from 35 solar radii (RS) at the beginning of the mission to 9.86 RS at the end of the primary mission.

The PSP (Parker Solar Probe) mission conducted by NASA is expected to significantly alter our understanding of the Sun. The PSP mission is expected to provide novel insights into solar events and activity, thereby enhancing our ability to forecast consequential space-weather events that impact human life on our planet. The Parker Solar Probe was launched by NASA with the aim of exploring the corona and safeguarding a civilization that is increasingly reliant on technology from the perils of space weather. The primary scientific aims of the mission are to cartographically represent the understanding of the heating of the solar corona, the flow of energy, and to examine the mechanisms that accelerate the solar wind. The Parker Solar Probe offers a statistical analysis of the outer corona.

Parker Solar Probe has three specific scientific goals.:

- (1)Determine the magnetic and plasma fields' structure and behaviour at the solar wind's sources.
- (2)Trace the energy flow that heats and accelerates the solar wind and corona.
- (3)Examine the processes that cause energetic particles to accelerate and move.

The Parker Solar Probe operates in harsh circumstances while collecting data in the Sun's corona and passing by our star more closely than any previous probe. Its four instrument suites, each specifically engineered to endure the extreme radiation and temperatures they will experience, define the dynamic area near to the Sun by monitoring particles as well as electric and magnetic fields.

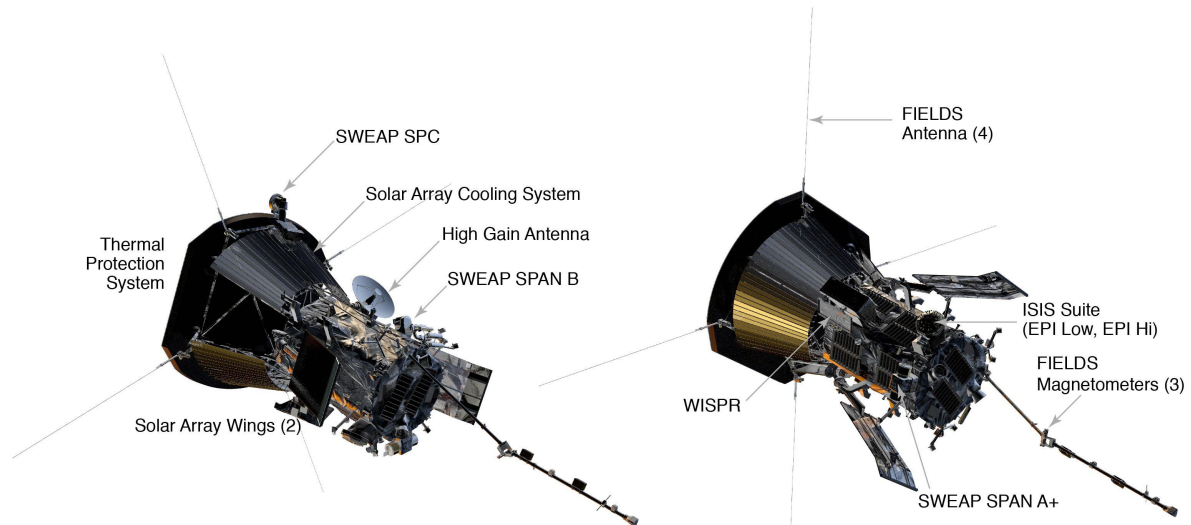


Figure 1.4: Parker Solar Probe Instrument

FIELDS

This instrument detects the scale and shape of magnetic and electric fields, radio emissions, and shock waves travelling through the plasma around the Sun. This device also functions as a massive dust detector, detecting voltage traces when tiny particles of space dust contact the antenna of the spacecraft.

FIELDS has five antennas to measure the electric field all over the spacecraft, 4 of which extend past the heat shield and into the visible area of Sun , where they may reach temperatures of 2,500 degrees Fahrenheit. The two meter long antennas are made by the niobium alloy that can tolerate incredibly high temperatures. It keeps track of electric fields remotely, on-site, and over a broad frequency range. The two modes of operation of the four antennas allow them to take observation of the properties of the slow and fast solar wind, the steady stream of solar particles that emerges from the Sun. The 5th antenna, which extends perpendicular to the others under the shadow of the heat shield, is employed to provide a 3-d representation of the electric field for higher frequencies.

FIELDS measures magnetic field by using 3 magnetometers, each roughly the size of a fist. The magnetic field is monitored using a search coil magnetometer, or SCM. It is feasible to trace the variations in the magnetic field by measuring the voltage that changing magnetic fields cause to occur in the coil. The large scale coronal magnetic field is picked up by the twin fluxgate magnetometers. The search coil magnetometer is required close to the sun because the magnetic field there is prone to fast change and it can examine the magnetic field at a rate of 2 million times/second. For measuring the magnetic field far away from the Sun, where MF(magnetic fields) fluctuates more slowly, fluxgate magnetometers are designed for this.

SWEAP

In order to gather data for the Solar Wind Electrons Alphas and Protons research(SWEAP), two tools are used: the Solar Probe Cup (SPC) and the Solar Probe Analyzers (SPAN). The instruments measure parameters like velocity, density, and temperature as well as count the most common solar wind particles including protons , electrons, and helium ions in order to fully understand the coronal plasma and solar wind. SPC is a metal object that can collect charged particles in a vacuum and is commonly referred to as a Faraday cup. The cup is peeked over the heat shield of spacecraft and revealed to the full sunlight, energy and heat of the Sun to see the passage of ions and electrons. The cup is made up of many collection plates that monitor the characteristics of the particles and a succession of extremely transparent grids, one of which sorts the particles using varied high voltages. The varying voltage grid helps to reduce unwanted noisy data, such as photo-ionized electrons and cosmic rays. The grids, which are found close to the instrument's front, may reach temperatures of 3,000 F and glow red while the equipment takes readings. The device isolates several components inside the cup electrically using chunks of sapphire. SPC makes up to 146 measurements each second as it approaches the Sun in order to precisely monitor the plasma's velocity, density, and temperature. Two devices make up SPAN, SPAN-B and SPAN-A. They have expansive fields of view that enable them to perceive regions of space that SPC is unable to monitor. When a particle hits a detector, It then enters a labyrinth, where the particles are separated based on their mass and charge by passing through a sequence of deflectors and voltages. Unlike SPAN-B, which only measures electrons, SPAN-A contains two components to monitor both ions and electrons.

Name	Type	Particle Measured	Measurement Type	Look Direction
SPAN-Ai	Electrostatic Analyzer + ToF	Ions	3D VDF + mass	Ram
SPAN-Ae	Electrostatic Analyzer	Electrons	3D VDF	Ram
SPAN-Be	Electrostatic Analyzer	Electrons	3D VDF	Anti-Ram
SPC	Faraday Cup	Ions and Electrons	1D VDF + energy-dependent flow angles	Nadir

Figure 1.5: SWEAP device

ISIS

Two complementary instruments are used by the Integrated Science Research of the Sun (IS-IS), which is called "ee-sis" and has the Sun's sign in its composition, to track particles at varying energies. By observing ions , electrons and protons. IS-IS will be

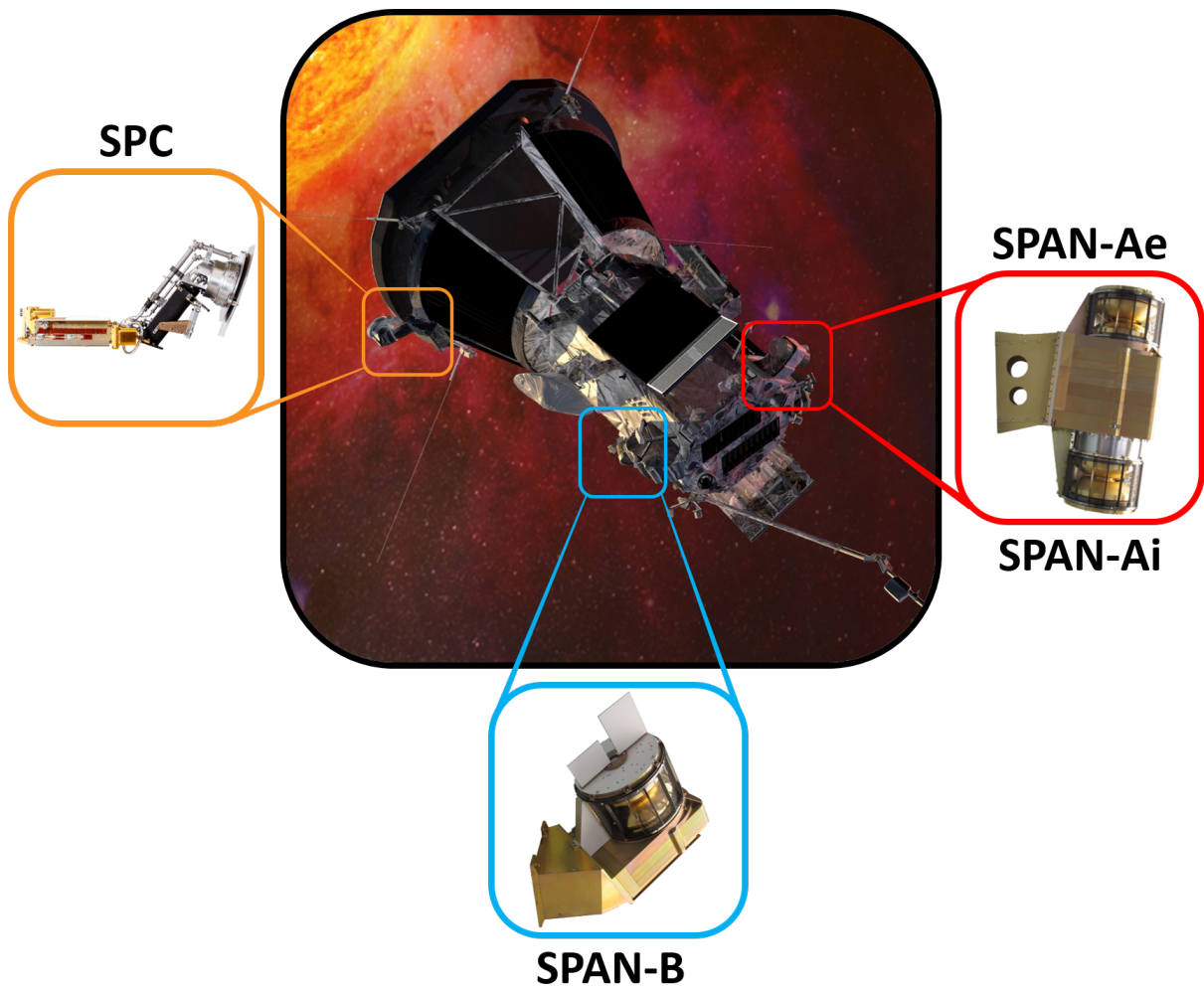


Figure 1.6: SWEAP suits four sensors

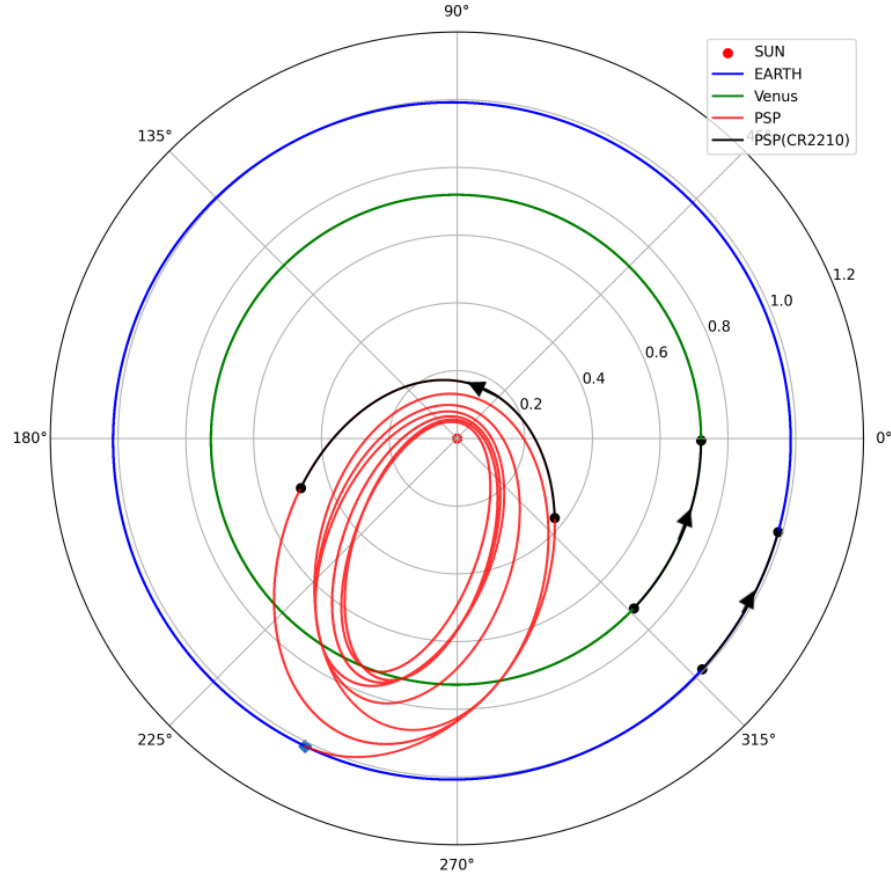
able to comprehend the particle lifetimes, such as where particles began, how particles were propelled, and also how left the Sun via interplanetary space. TEPI-Lo and EPI-Hi are the names of the two energetic particle detectors aboard ISIS (EPI stands for Energetic Particle Instrument). EPI-Lo analyses the spectra of ions and electrons to determine the presence of two isotopes of helium, He-3 and He-4, as well as carbon, oxygen, neon, magnesium, silicon, and iron. By differentiating between helium isotopes, it will be possible to figure out which of many proposed methods led to the acceleration of a particles. The device features an eye-catching sea urchin-like outline, with an octennial dome body that houses 80 dime-sized viewfinders. Various viewfinders give a broad field of vision for the detection of particles which have low energy. Through one of the viewfinders, a carbon polyimidee aluminum ion enters EPI-Lo. It then passes via two of that foils before coming into contact with a solid state detector. When the foils hit , electrons are produced, and a micro - channels plate uses these electrons to detect the energy. The energy from the ion-detector collision and the time it takes for the ions to flow through the sensor are used to determine the particle class. EPI-Hi employs 3 particle sensors made of stacked layers of detectors to observe particles with energy greater than those observed by EPI-Lo. The initial few layers employ geometrically segmented ultra fine silicon detectors to help reduce noise of background and establish the path of the particles. level to which charged particles enter the stack of detectors is measured, and charged particles are identified, through ionisation(It is the mechanism by which charged particles extract electron from an atom in individual detectors). When spacecraft is closest to the Sun, it(EPI-Hi) would be capable of detecting the particles up to 100k particles per second. Together, these two sensors allow ISIS to study both high-energy solar wind particles that SWEAP is unable to detect as well as solar energetic particles of all energies.

WISPR

WISPR full name is Wide Field Imager. It serves as the sole imaging tool present on board the mission. WISPR analyses the large-scale structure of the solar wind and corona before the spacecraft crosses them. The little WISPR equipment monitors solar ejection material from a distance, including jets , solar flares and CMEs, and other structures. As these formations travel away from the Sun and eventually pass over it, the other sensors on the spacecraft make in-situ observations of them. WISPR helps make the complex physical measurements being made right now in the solar region related to what is going on in the massive coronal structure. WISPR employs the shield of heat to hide the majority of Sun's radiation, which would differently obscure the much faint corona, in order to picture the solar atmosphere. Any stray light that is still present after being diffracted or reflected off the heat shield or other surfaces of the spaceship is dispersed and absorbed by specially made baffles and occulters. WISPR makes use of 2- radiation-resistant active pixel sensor CMOS cameras. Traditional CCDs are replaced by these detectors due to their lower power consumption and less weight. In addition, they are less susceptible to cosmic radiation and some other high-energy particles, that are a big concern in the solar system's proximity and can have damaging impacts. The lens material utilised in the camera is radiation-hard BK7 glass, which is often used in space telescopes and is suitably resistant to withstand impacts from dust.

In this work we plotted the trajectory of Parker Solar probe in the Heliocentric inertial

frame with Earth and Venus . See figure 1.7 In figure1.7 ,the red part is the whole journey of PSP ,red square is the starting point of PSP. The green and blue lines are the trajectory of venus and Earth respectively during the CR2210. Highlighted black part is trajectories during CR2210 .



Timeline: 2018-8-12 to 2025-6-19

Figure 1.7: Parker Solar Probe Trajectory

The following information is essential to understanding NASA’s historic mission to touch the Sun:

(1)The Parker Solar Probe represents the inaugural NASA mission to be designated after an individual who is currently alive, namely Eugene Parker. Despite the initial conception of the mission dating back to 1958, it took six decades for the requisite technological advancements to be realized. As previously mentioned, the spacecraft is equipped with groundbreaking technology. The Parker Solar Probe achieved a significant milestone by approaching the Sun’s surface at a distance of 26.55 million miles (42.72 million kilometres) within a few months of its launch. The object in question attained the highest velocity ever achieved by human beings, clocking in at 153,454 miles per hour. Subsequently, the aforementioned records have been surpassed on multiple occasions. In the year 2024, it is projected that the spacecraft will traverse a distance of 3.9 million miles (6.2 million kilometers) from the Sun’s surface at an approximate velocity of 430,000 miles per hour (700,000 kilometers per hour).

(2)The Parker Solar Probe successfully traversed the Alfvén critical surface, which marks the boundary at which solar material adhering to the Sun is released and forms the solar wind, during its initial entry into the solar atmosphere. This achievement represents the first instance of such a crossing. The appearance of the barrier prior to this crossing was unknown to all. The Parker Solar Probe conducted multiple transits through the corona during its initial approach, reaching a proximity sufficient to traverse the boundary. The formation of the Alfvén critical surface was non-spherical, yielding significant insights into its boundary morphology. On the contrary, the surface exhibits a series of spikes and troughs, resulting in a wrinkled appearance. The SWEAP sensor identified that the wrinkles were caused by the coronal streamers, which are massive plumes of solar material that rise through the Sun's atmosphere. The Parker Solar Probe successfully traversed the Alfvén critical surface, which represents the boundary at which solar material adhering to the Sun is released and forms the solar wind, during its initial foray into the solar atmosphere. This marks the first instance of such an achievement. The SWEAP sensor has identified that the wrinkles are attributed to the coronal streamers, which are vast columns of solar material that rise through the Sun's atmosphere. Streamers have been observed by spacecraft in close proximity to the Sun, however, direct measurements of these phenomena have yet to be conducted. The discoveries are modifying our comprehension of the atmosphere of the Sun and its transformation into the solar wind.

(3)During its journey to the Sun, Parker Solar Probe transmitted back initial findings indicating the presence of switchbacks, which are rapid changes in the Sun's magnetic field direction that resemble the pattern of a zig-zagging mountain road. This discovery was made by scientists analyzing magnetic field readings. Subsequently, FIELDS has provided aid in determining their source. The FIELDS data revealed a correlation between the switchbacks and magnetic "funnels" present in the solar surface, as observed during the sixth flyby of the Sun by the Parker Solar Probe. Supergranules are funnel-shaped formations on the surface of the Sun that are formed as a result of the rising, spreading, cooling, and falling of heated plasma from the solar core. The magnetic configurations of these regions suggest that the propulsion of the solar wind is attributed to magnetic reconnection.

The generation of switchbacks remains a subject of ongoing research, despite recent discoveries that have identified their specific locations. During its seven-year mission, the Parker probe is scheduled to make a minimum of seven passes in close proximity to the Sun. In 2024, it is anticipated that the celestial body in question will establish a new record for proximity to the Sun.

1.5 Space Weather Forecasting Models

During the recent 20 years, a large variety models of solar-wind with various methodologies were developed, with the mostly of them attempting to estimate the background solar wind at the Earth. ENLIL([Odstrčil and Pizzo, 1999](#)), SWMF ([Tóth et al., 2005](#)), and EUHFORIA([Pomoell and Poedts, 2018](#)) are examples of 3D MHD physics-based models that may provide us physical insight and supply us with data on the density, proton temperature of the solar wind and magnetic field of the sun. Some of the models use physics-based techniques like ENLIL or MHD about a Sphere ([Linker et al., 1999](#)) as

input, as well as integral synoptic photospheric magnetic field images. Empirical relationships between measured and observed Coronal holes areas and observed solar wind speeds at Earth(1 AU) ((Rotter et al., 2012); (Bussy-Virat and Ridley, 2014);(Vršnak et al. (2007); (Riley et al., 2017); (Owens et al., 2017);(Reiss et al., 2016)) are also used. Simple persistence models rely on in-situ data that are pushed forward in time based on the spacecraft's position. Some models employ MHD codes in the heliospheric and coronal regions, whilst others employ the WSA model(Arge and Pizzo, 2000) in the coronal regions and MHD codes in the heliospheric regions. In compared to real data, the completion of the various solar wind models show typical RMSE(root mean square errors) of roughly 100 to 150 km/s in solar wind velocity and temporal change in peak speed arrival of around one day and up to three days. Model performance often degrades as solar events and activity phases rise, as CMEs commonly disrupt interplanetary region. Empirical solar wind models, in particular, are incapable of dealing with such perturbations, but preconditioning is an essential consideration for numerical models as well.

1.6 Motivation

To meet the rising need for better predictions of space weather, a new model named SWASTi-SW (Space Weather Adaptive Simulation Framework for Solar Wind) was recently developed([Mayank et al., 2022](#))

PSP measures the in-situ properties of the solar wind along different radial distances. Due to which, it provides a special opportunity to check the efficacy of solar wind forecasting models.

The specific goals are as follows-

- To test the robustness of SWASTI, PSP data are assessed using SWASTi and model data are compared with psp observed data.
- To understand the dynamical properties of solar wind And predict solar wind velocity at inner heliosphere.

In chapter-2 we explain theoretical aspect about our work and introduce SWASTi-SW with its default parameters. Chapter-2 also describe used coordinate systems. Chapter-3 deals with methodology and data products of PSP. Chapter-4 deals with the validation of the model results with in-situ measurement and addresses some restrictions of the basic setup of SWASTi-SW. In chapter 5 we summarize our results.

Chapter 2

Theoretical Aspect

2.1 Parker's Solar Wind

University of Chicago's young professor named Eugene Parker made a discovery that altered our knowledge of all stars, including the Sun, about 70 years ago. The solar wind is a steady flow of solar wind particles that make up the solar corona, or atmosphere of the Sun. Prior to Parker's discovery in 1958, several researchers speculated that the solar wind may exist based on comet back ends observations , but no one had performed the calculations necessary to conclusively prove its existence.

Parker's investigation was primarily focused on two issues: what, if anything, accelerates a gas moving away from the Sun to outer space, and how does this gas movement affect the solar magnetic field's structure when it is far from the Sun? He first used factors that had been measured to compute the flow of kinetic energy , or the rate at which the solar corona at Earth transfers kinetic energy across a surface. For the purpose of examining the solar wind's dynamics, the reference point is the flow of kinetic energy at the Earth. Parker also established a few presumptions that served as the basis for his derivations. He did this by treating the Sun like a solid sphere and originally ignoring the solar magnetic field's role. He also established the radius a , which is depicted in Figure 2.1 as the boundary between the inner and outer solar corona.

Parker then gave thought to a situation in which the gas around the Sun is in fixed equilibrium, meaning that all of the forces acting on it are equal to zero. Parker created equations for the pressure and density of the solar wind based on this supposition. He discovered that the density was 0 at an indefinite distance from the surface of Sun, which is consistent with the interstellar region space's predicted density. Parker came to the conclusion that the solar corona is not fixed but rather expanding since the predicted pressure was significantly lower than the pressure that was anticipated at great distances.

Parker then determined the characteristics of solar wind based on the theory that the corona is expanding steadily. This presumption necessitates the consideration of a few more factors. The corona's heating process and its internal heating distribution, in particular, were unknown factors. Parker made the assumption that the corona's temperature distribution was understood in order to take this into consideration. He arrived at equations for the velocity profile which was for the corona. He discovered that an expanding corona produced suitable amounts of pressure and density at distances away from the Sun by demonstrating that these equations held for numerous dimensions.

Parker continued his investigation on the heating of an expanding corona after establishing its growth. Consider the heating process with the boundary condition being

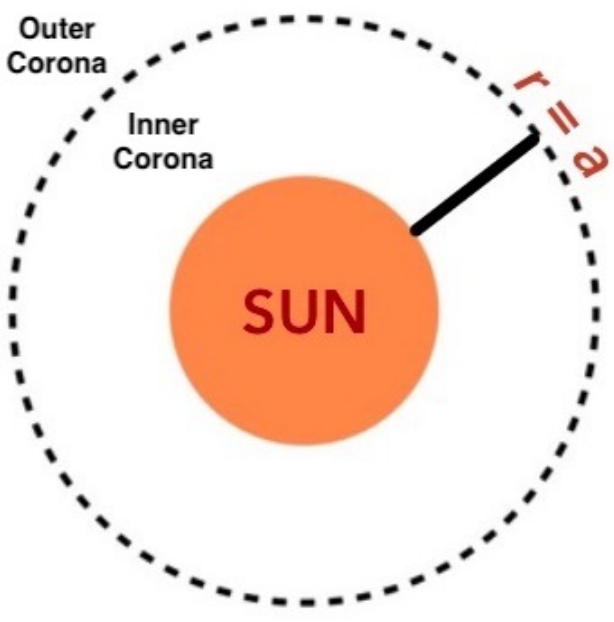


Figure 2.1: The distance, a , between the inner and outer solar corona.

the kinetic energy flux at Earth. The needed temperature and quantity of mass loss were found to be compatible with the expected values at Earth. He therefore assumed a mechanical heating process, i.e. heating by hydrodynamic waves. Parker came to the conclusion that the corona is certainly growing and is being heated by an unknown process as a result. Parker also thought about how a magnetic field would affect the corona's



Figure 2.2: The Parker Spiral, a solar magnetic field arrangement at far distances from the Sun.

expansion. The movements of the outflowing material can alter magnetic fields because it is a plasma, a totally ionised gas. Parker was interested in understanding how the arrangement of the solar magnetic field at a great distance might be impacted by a growing corona. He concluded that the magnetic field would be totally radial for a stationary Sun. But the Sun is a star that revolves. Parker found that under these circumstances, the increasing solar wind spirals the solar magnetic field at great distances. The Parker spiral is the current name for this arrangement.

Parker showed through his derivations that the solar wind should exist, even if his models weren't validated until 1962. A number of missions are now in progress to try to find the answers to some of the major issues Parker asked, some of which are still open to this day. Even yet, there are still many things about this work that solar and stellar astronomers should be grateful for.

2.2 Stellar winds

Stellar winds are the quickly moving streams of protons, electrons, and heavier metal atoms that are released by stars. Continuous outflows of material flowing at rates ranging from 20 to 2,000 km/s define these winds. On the Sun, the wind blows from quiet areas at a speed of 200–300 km/s and from coronal holes and active regions at a speed of 700 km/s.

Stellar winds have different sources, ejection rates, and velocity depending on the star's mass. The wind is brought on by the corona's exceptionally high temperature (millions of degrees Kelvin) in low-mass, comparatively cold stars like the Sun. The coronal gas has enough energy to leave the star's gravitational pull as a wind thanks to this high temperature, which is hypothesised to be caused by interactions between magnetic fields at the star's surface. Although stars of this class only release millions of tonnes of material each second and only a minor percent of their mass is lost annually as a stellar wind (for instance, just 1 part in 10^{14} of the Sun's mass is lost annually), this nevertheless constitutes material losses. Only a very small portion of 1 percent the mass of stars like our Sun is lost by stellar winds over the course of their entire existence.

The stellar winds of hot, massive stars, however, can be a billion times more powerful than those of low-mass stars. They may release large amounts of material in the form of 2,000 km/sec winds during the course of their brief lives, possibly up to 50 percent of their starting mass. Direct radiation pressure from photons departing the star drives these stellar winds. High-mass stars occasionally have the ability to almost completely expel their outer envelopes in winds. We get a Wolf-Rayet star as a consequence. Massive stars like the Wolf-Rayet Star are rapidly shedding mass as they reach an advanced stage of stellar development.

2.3 Coordinate System

Unlike ground-based observatories and satellites in Earth orbit, spacecraft use a different approach to viewing the Sun. Additionally, because it is a gaseous body, the Sun lacks any stable points of reference. The Sun's distinct parts also rotate at varying rates. The strength of the magnetic field lines anchored in the photosphere of a particular feature affects the rotation rate in addition to latitude. So for the comparison with earth based

observatories data there are different coordinate system which is called Spacecraft coordinate system.

2.3.1 Spacecraft Coordinate System

So most of the spacecraft data are in the Radial Tangential Normal (RTN) coordinate system and our model gives the output in spherical coordinate system. PSP data also in RTN format that's why for the comparison of model and observed data we had to convert both data in one coordinate system so we can compare it easily. We convert PSP data from RTN to HEEQ and then HEEQ to Stonyhurst. Similarly modeled data from spherical to cartesian, cartesian to HEEQ and then HEEQ to Stonyhurst. In the end we have both data in the same coordinate system.

By including the radial distance(r) from the Sun's centre, the well-known heliographic coordinate system, which expresses a feature on the solar surface's latitude and longitude, may be extended to three dimensions. The heliographic coordinate system has two fundamental variations. Carrington heliographic system and Stonyhurst heliographic coordinate ([Thompson, 2006](#)). Both have the same solar rotating axis; the only difference is how longitude is defined.

Stonyhurst Heliographic Coordinate

The Stonyhurst heliographic coordinate system was developed at the point where the central meridian and solar equator meet as seen from Earth.

Heliocentric Earth Equatorial Coordinate (HEEQ)

The XHEEQ axis in HEEQ coordinates points at the intersection of the central meridian and solar equator as seen from Earth, whereas the ZHEEQ axis is parallel to the solar North rotation pole.

Heliocentric cartesian coordinate

The coordinate system in question is oriented towards the right-hand side. The Cartesian coordinate system denoted by (x, y, z) exhibits perpendicularity among all its axes and parallelism among all lines of constant y (or x , or z). The z -axis is interpreted as being parallel to the line connecting the observer and the Sun, and is oriented in the direction of the observer. The y -axis is perceived as being orthogonal to the z -axis and situated in the plane that encompasses both the z -axis and the axis of the solar North pole. The y -axis ascends towards the solar North pole. The x -axis is oriented orthogonally to both the y -axis and the z -axis, whereby the positive direction of the x -axis is aligned with the solar West.

R-T-N

For many interplanetary missions, the Radial-Tangential-Normal heliospheric reference frame is employed (e.g. Voyager, Helios, Ulysses, STEREO). The local velocity and magnetic field vectors may be easily expressed in this cartesian frame. The R basis vector in this coordinate system is orientated to point from the sun along the spacecraft-sun line, toward the current location of the Parker Solar Probe. The cross product of the

solar rotation axis and R yields the T basis vector, and the N basis vector completes the triad.

2.3.2 Coordinate conversion

Heliocentric Earth Equatorial (HEEQ) coordinates and Stonyhurst heliographic coordinates have a close relationship. The equations below provide a conversion between these two systems: **HEEQ to Stonyhurst :-**

$$r = \sqrt{X_{HEEQ}^2 + Y_{HEEQ}^2 + Z_{HEEQ}^2} \quad (2.1)$$

$$\Theta = \tan^{-1} \left(\frac{Z_{HEEQ}}{\sqrt{X_{HEEQ}^2 + Y_{HEEQ}^2}} \right) \quad (2.2)$$

$$\Phi = \arg(X_{HEEQ}, Y_{HEEQ}) \quad (2.3)$$

Stonyhurst to HEEQ:-

$$X_{HEEQ} = r \cos \Theta \cos \Phi \quad (2.4)$$

$$Y_{HEEQ} = r \cos \Theta \sin \Phi \quad (2.5)$$

$$Z_{HEEQ} = r \sin \Theta \quad (2.6)$$

The conversion between heliocentric Earth Equatorial ($X_{HEEQ}, Y_{HEEQ}, Z_{HEEQ}$) and heliocentric Cartesian (x, y, z) as seen from Earth follows:

Heliocentric Cartesian to HEEQ:-

$$X_{HEEQ} = z \cos B_0 y \sin B_0, \quad (2.7)$$

$$Y_{HEEQ} = x, \quad (2.8)$$

$$Z_{HEEQ} = z \sin B_0 + y \cos B_0, \quad (2.9)$$

HEEQ to Heliocentric Cartesian:-

$$x = Y_{HEEQ}, \quad (2.10)$$

$$y = \cos B_0 Z_{HEEQ} - \sin B_0 X_{HEEQ}, \quad (2.11)$$

$$z = \sin B_0 Z_{HEEQ} + \cos B_0 X_{HEEQ}, \quad (2.12)$$

2.3.3 Magnetogram

A magnetogram is a two-dimensional picture that shows the direction and strength of the magnetic field on the solar photosphere, or the visible surface of the Sun. For the study of solar activity and its effects on space weather, magnetograms are a crucial instrument. Specialised solar telescopes fitted with sensors that can detect the Sun's magnetic field are used to create magnetograms. These instruments utilize the Zeeman effect, a phenomenon where the presence of a magnetic field causes the splitting of spectral lines in the light emitted by atoms or ions. There are many observatories continuously observing the Sun. It is to be noted that one can only measure the line of sight components of solar magnetic field by the above method. The data obtained from these observatories are given in the form of Synoptic map for a particular Carrington Rotation.

Carrington Rotation

Sun is in a differential rotation, which means that different latitudes have different time periods of rotation, but if we fix a frame that is rotating with a time period that is close to the Sun's rotation period (in some sense, if the differential rotation is not so significant), we can map the Sun's surface in that frame. This rotating frame is called Carrington frame, and each Carrington rotation is given a number called Carrington Rotation. A Carrington rotation is of 27.2753 days. For example, CR 2210 used in the present study has observation data from 23 October to 26 November 2018.

Synoptic map

Synoptic maps represent the Sun's photospheric magnetic field in a two-dimensional format, which is dependent on heliographic latitude and Carrington longitude. The terms "synoptic charts" or "synoptic magnetograms" are commonly used to refer to these entities. The provided data presents a comprehensive analysis of the magnetic field of the Sun over the course of a complete solar rotation, which spans approximately 27 days as observed from Earth.

Synoptic maps are constructed by combining a number of magnetograms, which are measurements of the Sun's magnetic field recorded over the course of one solar revolution at various longitudes. Magnetograms are collected at various Carrington longitudes and then projected onto a rectangular grid as the Sun revolves. A full picture of the Sun's magnetic field distribution is produced as a consequence, which is necessary for comprehending solar activity and how it affects space weather.

GONG (Global Oscillation Network Group)

The Global Oscillation Network Group (GONG) produces synoptic maps of the Sun's photospheric magnetic field by combining a series of magnetograms obtained over a solar rotation. The magnetic fields on the solar surface is derived from the line-of-sight magnetic fields assuming that the field is approximately radial at the solar surface. Its data is taken at 676.8 nm and on equally spaced grids in $\cos\theta$ and $\phi(180 \times 360)$, mapped on the Solar surface, for a particular Carrington rotation (cr). Here's an outline of how GONG produces synoptic maps:

- 1. Magnetogram acquisition:** GONG operates a network of six ground-based observatories distributed around the globe, ensuring continuous observations of the Sun.

These observatories collect magnetograms, which are measurements of the Sun's magnetic field.

2. Data processing: The magnetograms are processed to correct for any instrumental effects, such as noise or distortion, and to calibrate the magnetic field measurements.

3. Map construction: As the Sun rotates, magnetograms are obtained at different Carrington longitudes. These magnetograms are then assembled into a synoptic map, which provides a global view of the Sun's magnetic field over a full solar rotation. The magnetograms are projected onto a rectangular grid of heliographic latitude and Carrington longitude, creating a synoptic map that spans from -90 to 90 degrees latitude and 0 to 360 degrees longitude.

WSO (The Wilcox Solar Observatory)

The maps from WSO also follow the same pattern, but it has 30 data points of equal separation in sine latitude, and equally spaced points separated by 5 degrees in longitude. The magneto-gram data from WSO provides both line of sight as well as the radial magnetic field measurements.

HMI (Helioseismic and Magnetic Imager)

Using information from 20 magnetograms taken around the central meridian, HMI Carrington Rotation synoptic maps are produced. There are two sizes for line-of-sight and inferred radial synoptic maps: 3600*1440 and 720*360. 720s HMI magnetograms are used to create final maps following the Carrington Rotation. Every 24 hours, daily maps are updated with the most recent nrt information within 60 degrees of CM.

ADAPT (Air Force Data Assimilative Photospheric flux Transport)

The ADAPT (Air Force Data Assimilative Photospheric flux Transport) model is a data-driven model used to create synoptic maps of the Sun's photospheric magnetic field. It combines observational data with a flux transport model to produce synoptic maps that include far-side observations and evolving magnetic features. Here's an outline of how the ADAPT model creates synoptic maps:

Data assimilation: The ADAPT model takes as input the available photospheric magnetic field data, such as magnetograms from observatories like the Solar Dynamics Observatory (SDO), the Global Oscillation Network Group (GONG), or the National Solar Observatory (NSO). This data provides information about the Sun's magnetic field on the Earth-facing side (near-side).

Far-side observations: The ADAPT model can also incorporate far-side (non-Earth-facing side) magnetic field information obtained through helioseismic imaging techniques, such as helioseismic holography or time-distance helioseismology. This data helps to fill in the gaps in magnetic field information for the far-side of the Sun.

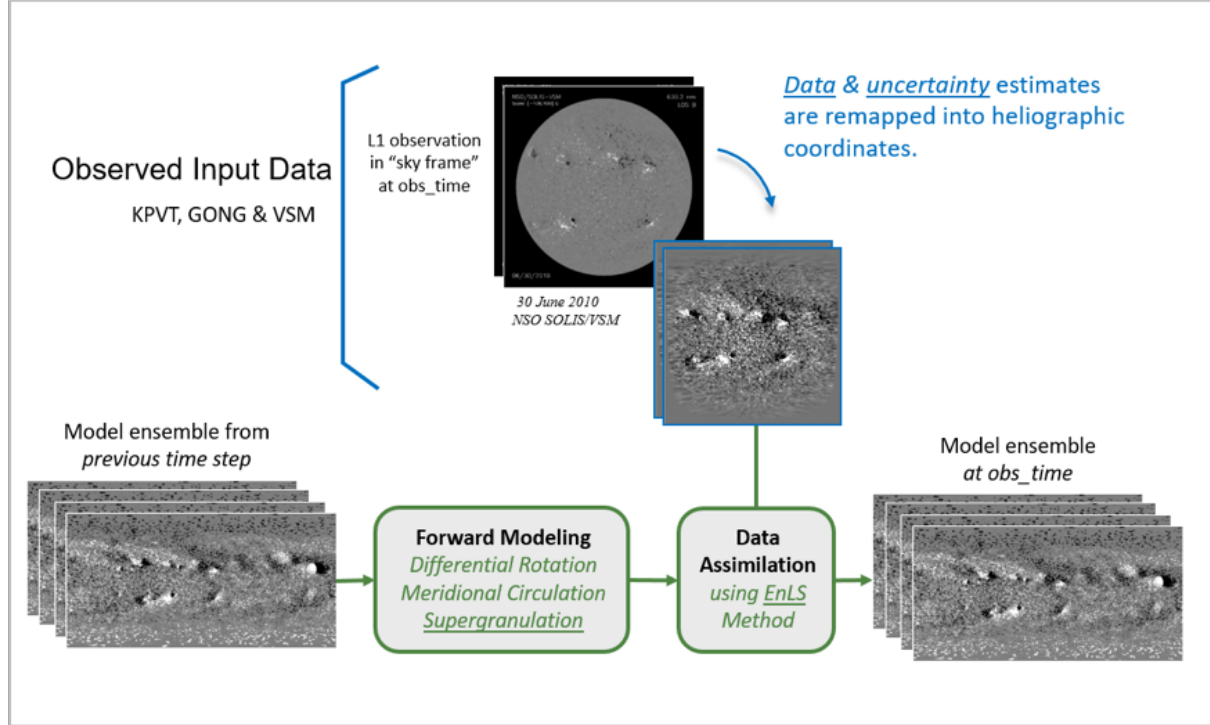


Figure 2.3: The general ADAPT model framework

Flux transport model: The ADAPT model utilizes a photospheric flux transport model to replicate the progression of the magnetic field on the surface of the sun. The aforementioned model takes into account multiple processes, including differential rotation, meridional flow, and the turbulent convection-induced diffusion of magnetic flux. Through the integration of these procedures, the ADAPT framework has the capability to forecast the progression of the Sun's magnetic field over a period of time.

Data assimilation and model update: The ADAPT model continuously assimilates new magnetogram data and updates the flux transport model as new observations become available. This allows the model to adjust its predictions based on the latest magnetic field measurements, ensuring the most up-to-date and accurate synoptic map.

Synoptic map creation: As the ADAPT model assimilates magnetogram data and evolves the magnetic field using the flux transport model, it builds a synoptic map that spans a full solar rotation. The final synoptic map represents the distribution of the Sun's magnetic field as a function of heliographic latitude and Carrington longitude.

The ADAPT model can produce ensemble maps to account for uncertainties and variations in the photospheric magnetic field data and to assess the robustness of the magnetic field predictions. An ensemble is a collection of model simulations, each generated using slightly different initial conditions or model parameters. The ensemble approach helps to quantify the uncertainties in the forecast and improve the overall prediction accuracy.

When the ADAPT model produces 12 ensemble maps, it creates 12 different synoptic maps with varying initial conditions or model parameters. These variations can include small changes in the input magnetograms, the incorporation of far-side data, or adjustments to the flux transport model parameters.

By comparing the ensemble maps, researchers can assess the consistency of the magnetic field predictions and the sensitivity of the model to the input data and parameters. Areas where the ensemble maps show significant agreement can be considered more reliable predictions, while areas with larger differences indicate greater uncertainty in the magnetic field forecast.

Difference between GONG and ADAPT:

The main difference between the ADAPT and GONG magnetograms lies in the method used to create the synoptic maps:

Data-driven vs. data assimilation: GONG magnetograms are data-driven, meaning they are constructed purely from observational data. GONG synoptic maps provide a direct representation of the photospheric magnetic field as observed from Earth over a solar rotation. In contrast, the ADAPT model uses data assimilation, incorporating both observational data and a flux transport model to create synoptic maps. This allows ADAPT to include far-side magnetic field information and simulate the evolution of the magnetic field over time.

Ensemble maps: The ADAPT model can produce ensemble maps by running multiple simulations with varying initial conditions or model parameters. This approach helps to quantify uncertainties and assess the robustness of the magnetic field predictions. GONG does not produce ensemble maps as part of its standard synoptic map creation process.

In summary, the main differences between ADAPT and GONG magnetograms lie in the methods used to create synoptic maps. GONG relies solely on observational data, while ADAPT uses data assimilation with a flux transport model. Additionally, the ADAPT model can produce ensemble maps, while GONG does not have this capability as part of its standard process.

2.4 MHD Model:- Space Weather Adaptive Simulation Framework for Solar Wind (SWASTi-SW)

SWASTi-SW is a data-driven three dimensional physics based solar wind model. The two domain method serves as its foundation. the inner heliospheric region is based on MHD, while the coronal domain is semi-empirical.([Mayank et al., 2022](#)) By using input from the coronal model, establishing the plasma characteristics in the inner heliosphere is the major aim of the MHD based inner heliospheric model. using the photospheric magnetogram as a data source to calculate the plasma properties in the inner heliosphere, Figure 2.3 depicts the steps taken by SWASTi-SW. The coronal domain's geographical range is $1.0\text{-}21.5R_s$ (0.1 au), while the inner heliosphere's range is 0.1-2.1 AU. The above scheme is also employed to simulate the connection of Sun Earth, as shown, for instance, in ENLIL, SUSANOO and EUHFORIA.

SWASTi-SW model uses the full-disk photospheric magnetogram as its only observational input. It is crucial to carefully select the right kind of input magnetogram as

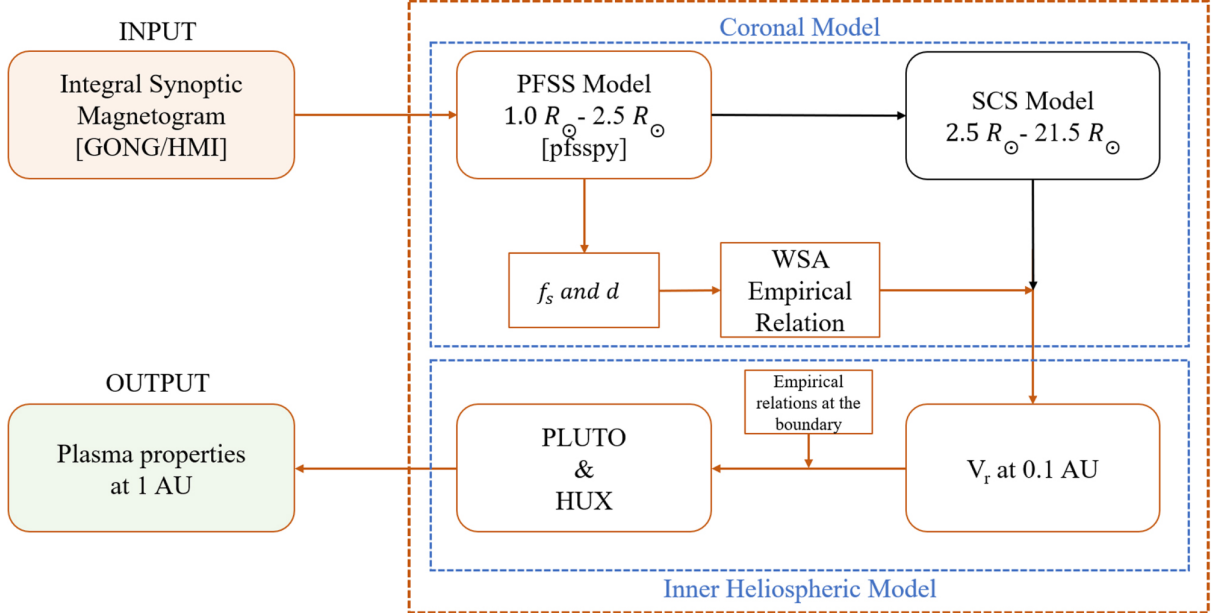


Figure 2.4: The suggested solar wind model’s process flow diagram displays the variety of numerical models used in the subdomain. ([Mayank et al., 2022](#))

a result. This model utilised the Helioseismic and Magnetic Imager (SDO) and NSO-integrated GONG’s Carrington rotation (CR) synoptic maps (filename prefix: mrmqs) (HMI). In order to calibrate the integral synoptic maps, conventional line of sight (LOS) maps are combined and remapped into the carrington frame with proper longitude. The synoptic map involves the utilization of a weighting factor to average standard magnetograms at the central meridian of each Carrington longitude. For additional information, see Scherrer et al (2012) and Hill (2018). The utilization of Integral CR synoptic maps provides a notable benefit in that each point along the x-axis (longitude) accurately depicts Earth’s location during the corresponding CR period. This feature facilitates the expeditious computation of the requisite data for the examination of the ambient solar wind in the inner heliosphere. It is necessary to perform coordinate system transformations to facilitate the comparison of in-situ measurements.

The plasma properties in the inner heliosphere will be established by utilizing an MHD-based model, which will be informed by data obtained from the coronal model. Accurate initial boundary conditions that heavily depend on the speed profile produced by the WSA relation are essential for the validity of this domain. The inner heliospheric model is founded upon the utilization of the Godunov-type PLUTO algorithm, which incorporates several conservation laws via a finite difference or finite volume approach. The current iteration of SWASTi-SW incorporates the optimal magnetohydrodynamic (MHD) module of PLUTO on a consistent, unchanging grid in spherical coordinates. The finite-volume approach is used to solve the following collection of conservative equations:

$$\frac{\partial \rho}{\partial t} + \nabla(\rho v) = 0 \quad (2.13)$$

$$\frac{\partial m}{\partial t} + \nabla \left[mv - BB + \left(p + \frac{B^2}{2} \right) \right] = \rho g \quad (2.14)$$

$$\frac{\partial B}{\partial t} - \nabla \times (v \times B) = 0 \quad (2.15)$$

$$\frac{\partial E_t}{\partial t} + \Delta \left[\left(\frac{\rho v^2}{2} + \frac{\gamma p}{\gamma - 1} \right) v + B \times (v \times B) \right] = mg \quad (2.16)$$

where v is velocity vector, ρ is mass density, m is momentum density (v), p is isotropic thermal pressure, $\gamma = \frac{5}{3}$ is specific heat ratio, g is gravitational acceleration ($-\frac{GM}{r^2}$), B is magnetic field vector and E_t is total energy density of solar wind plasma.

They solve the MHD equations in the Stonyhurst heliographic(SH) coordinate system. Using the spherical to Cartesian coordinate transformation, the coordinates of this frame may be converted into the Heliocentric Earth Equatorial (HEEQ) frame.(Thompson, 2006). In order to account for the spinning of the Sun in the SH frame, the entire spherical slice at R_{In} , which defines the inner radial boundary, is rotated by uniform angular velocity with regard to the computing grid. Depending on where the Earth is in its orbit, the rotating period of time (TP), which is constant for a given CR, can range from 27.21 to 27.34 days. In order to account for the rotation of the Sun in this frame, the entire spherical slice at R_{In} , which defines the inner radial boundary, is revolved with uniform angular speed with respect to the computation grid. The MHD domain range has a grid resolution of $150 \times 120 \times 360$ and ranges from 0.1 to 2.1 AU , -60 to +60° and 0 to 360° in the radial , latitudinal and longitudinal directions respectively . We used straightforward numerical techniques that are often used in a PLUTO TS (time step) cycle in order to keep the calculation time within practical bounds.

2.4.1 Comparing SWASTi-SW model Data from Omni Data at 1 AU(Past study)

This model already satisfy the plasma properties at L1 for following CR. More details ar in the. This model simulate the plasma properties for L1 and compare the data for omini database at 1AU near Earth. For CR2053 , the structure observed (rmse = 80.87 km/s and cc = 0.81),it features a global peak and two local side to side peaks in the middle of figure(2.4), has been accurately reflected by SWASTi-SW speed profile output. In figure 2.4 the speed profile of plasma of the above CRs at lagrange point 1(L1).OMINI hourly averages data are presented with the HUX and MHD values for CR2077, CR2053, CR2022 and CR2081 taking input from magnetogram of GONG. Along with MHD (INPUT-GONG), HUX, and OMNI data, MHDHMI (using HMI magnetogram) has also been displayed for CR2104. For the MHDGONG findings, which are displayed in blue, the PCC(Pearson Correlation Coefficient) and RMSE(Root Mean Squire Error) have been computed.

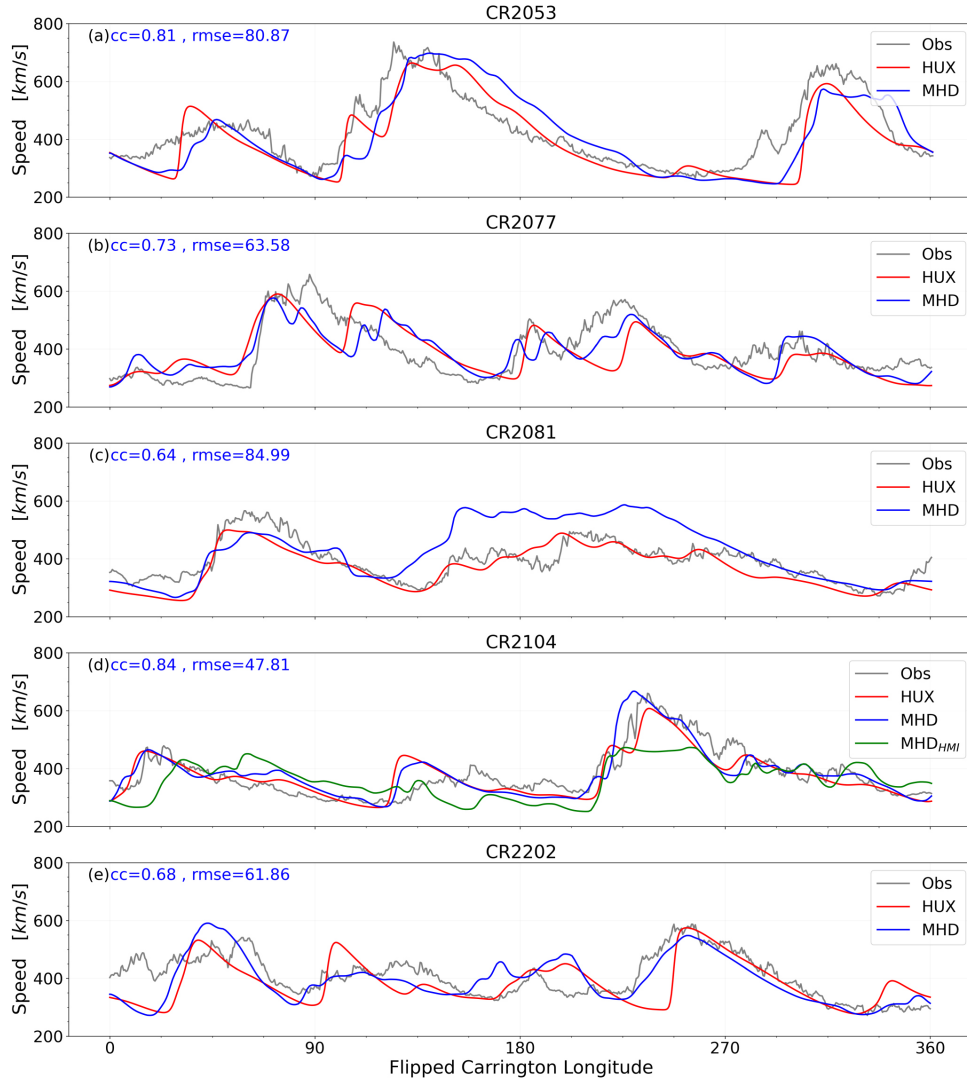


Figure 2.5: Plasma speed profile for the above CRs at L1. Image taken from ([Mayank et al., 2022](#))

Chapter 3

Methodology

We provide the initial SWASTi-SW findings for a few chosen CRs. The selected CR numbers, denoting the commencement month, comprise CR2210 (November 2018), CR2215 (March 2019), and CR2216 (April 2019). The Carrington rotation(CRs) are selected in order to cover the perihelion of the first and second orbits of the Parker Solar Probe (PSP), which fall within the concluding stage of solar cycle 24. The MHD region's spatial domain extends to 2.1 astronomical units, covering the territories of Mercury, Venus, Earth, and Mars. Figure 4.4 displays a visual representation of the output at a particular point in time.

We compare the model results with the in-situ measured plasma parameters as reported by the FIELDS experiment and Solar Wind Electron, Alphas and Proton Instrument to determine how well SWASTi-SW simulates the background solar wind. The model setup was made in accordance with the provided instructions and ran on a machine with 48 cores, which takes approximately 6.5–9.5 hours to compute the result for the chosen resolution. We present the SWASTi-SW findings for one CR in order to validate the output of SWASTi-SW model. The selected CR number is CR2210, and its dates are October 26, 2018, through November 23, 2018. For predicting the solar wind at the location of the Parker Solar Probe, we followed the following approach:

As previously discussed, the SWASTi-SW model has been developed in a manner that supports ease of use, as it is designed to be user-friendly. In this code, it is necessary to specify the time frame for which the plasma properties data is required. The program exclusively relies on GONG and HMI synoptic map input. However, I have devised a modification to enable its compatibility with ADAPT synoptic files. Subsequently, we utilized the Gong and Adapt model Synoptic maps data as input for a specific Carrington rotation and executed the model. The desired compression ratio and temporal resolution were specified. The complete Carrington Rotation(CR) measurement of plasma properties was obtained within the range of 0.1 AU to 2.0 AU, -60 to +60, and 0 to 360 in the radial, latitudinal, and longitudinal directions, respectively. Which have $150 \times 120 \times 360$ grid resolution, respectively. Then we compared the outputs of model with the observed velocity at the PSP in-situ data using CDAweb database.

We also compute the Pearson correlation coefficient (cc) and the Root Mean Square Error to statistically determine the best fit (rmse).

1. Pearson Correlation Coefficient

$$r_{xy} = \frac{\sum_{n=1}^n (x_i - \bar{x})(y_i - \bar{y})}{\sqrt{\sum_{n=1}^n (x_i - \bar{x})^2} \sqrt{\sum_{n=1}^n (y_i - \bar{y})^2}} \quad (3.1)$$

where :

- y_i, x_i , are the individual sample points indexed with i
- $\bar{y} = \frac{1}{n} \sum_{n=1}^n y_i$ (the sample mean); and analogously for \bar{x} .
- n is a sample size.

It shows how the observed and simulated values are co-related with each other.

2. Root Mean Square Error(RMSE):

$$RMSE = \sqrt{\frac{\sum_{i=1}^n (X_{obsi} - X_{modeli})^2}{n}} \quad (3.2)$$

Where:

- X_{obs} is observed value and X_{model} is modelled values at times i.

3.1 Data Products (PSP)

The probe collects data about plasma in the corona and sends it back to Earth for NASA researchers to study. Data of PSP from different instruments managed by different organizations. All organization upload the data on CDAweb portal so everyone in the world can use the data. We have used Sweap instrument data for the plasma properties like solar wind speed ,proton density and temperature. It mainly monitors solar wind thermal plasma. A faraday cup pointing at Sun, this equipment called the SPC(Solar Probe Cup) primarily monitors alpha particles and protons. Additionally, it is occasionally set up to detect electron. On both side of the spacecraft bus are electrostatic analyzers, which are a component of the instrument of SPC(Solar Probe Analyzer) . The Solar Probe Analyzers A ion is used to measure alphas, protons and other heavy ions. Electrons are measured using the Solar Probe Analyzer (A and B; SPAN-electron). If in any case one of the instrument is not working and the solar winds flow detection is not happened then other instrument can do this work since the SPC and SPAN devices fields of view are intended to overlap and be complimentary for full coverage.Generally speaking, SPC is optimal for flows parallel to shield of heat, and perpendicular to the probe Z-axis, whereas SPAN is intended for flows at broader angles. The Parker Solar Probe's main objective is to collect data while it is near 0.25 AU of the Sun during an orbit. Outside of this range, there have been some protracted campaigns. The data are provided for days when the instruments were active inside 1/4 AU as well as days when the instrument were operating outside of 1/4 AU(0.25AU).

There are different levels of data available from the Sweap instrument. Initial data is a raw data which is processed by different organization. All SWEAP data are labelled source_descriptor_datatype_YYYYMMDD_vVV, where month, year and day are shown by MM, YYYY, and DD respectively, and VV denotes the data release's version number. Each SWEAP data file contains a collection of measurements from one observation day

of a specific type. A self-documenting data structure is used to deliver measurements by a CDF (Common Data Format) file. . All CDF data files can access by the CDF software providing by NASA (<https://cdf.gsfc.nasa.gov>).

Level-2 ion: (psp_swp_spc_l2i_yyyymmdd_v01.cdf)

This data product contains observations of the ion charge flow as a function of energy/charge carrier (the barrier of voltage imposed on a number of transparent grids upstream of the sensor) are contained in this data product. The readings are grouped into spectra, each of which is made up of a series of ascending voltage steps that are sequential and increase in magnitude.

Level-3 ion: (psp_swp_spc_l3i_yyyymmdd_v01.cdf)

This data product includes calculated density and temperature measurements and velocity vector of the ions of solar winds. These measurements perfectly match the spectra from the same day's psp swp spc l2i file. In this data product, two methods are used to analyzed ion spectrum—moments and fits. Each approach yields an estimate of the ion population's density, temperature (thermal speed), and velocity vector. Two frames of reference are used for presenting velocity vectors: "RTN," which is an inertial RTN system, and "SC," which is the spacecraft reference frame.

3.2 Data collection

We have collected PSP data in different time resolution from different organization . We got the 1 hour time resolution data from Coordinated Data Analysis Web (CDAWeb). Selected non-solar heliophysics datasets from ongoing and completed heliophysics missions and initiatives are available on CDAWeb. SPDF only saves the most recent version of many datasets from ongoing missions because they are frequently (even daily) updated, including by reprocessing data from earlier time periods. Other than this we also have 1 minute magnetic field data and secondly cadence data for all plasma properties.

OMNI data from the SPDF COHOWeb database (<https://cohoweb.gsfc.nasa.gov/coho/>). The NASA SPDF (<https://spdf.gsfc.nasa.gov/>), COHOWeb (<https://spdf.gsfc.nasa.gov/>), the Science Operation Centers of the four science inquiry teams, and the APL Parker Solar Probe Gateway provided the PSP data used in this work.

Chapter 4

Results

4.1 Results:CR2210

4.1.1 Using Gong Magnetogram

Comparison with PSP data

The PSP spacecraft made its first visit to the Sun in November 2018 comes under CR2210, while it was immersed in slow wind stream that was coming from a tiny coronal hole([Badman et al., 2020](#)) ([Szabo et al., 2020](#))([Riley et al., 2019](#)) .

We used the same process as L1 to estimate wind velocity for another Carrington rotation CR2210 with input data from the GONG observatory to show the applicability of SWASTi-SW toolbox ([Mayank et al., 2022](#)) of solar wind. The first panel of figure 4.1 displays the modeled solar wind properties with the PSP measured properties.

Here we select Sweep suit's SPC plasma data and Fields instrument data [Kasper et al. \(2016\)](#)([Bale et al., 2016](#)), these data is in different resolution but for now we chose 1 hour time resolution for the CR2210. The plasma speed for the chosen CR at PSP is shown in Figure4.1. The SWASTi model's output has been compared in this figure to data that has been averaged over one hour using PSP. Since the observed speed of plasma is predominantly radial so it has been contrasted with the model's radial velocity. Number density, magnetic field and proton temperature are all presented in figure 4.1 for comparison with PSP data.

As the heliocentric distance steadily reduces to 0.1 au in the starting half period of CR2210 up to 2018/11/05, the model's radial magnetic field and velocity at PSP mostly vary between the negative 50 to positive 10 nT and 300-600 km/s ranges, respectively. The model's radial magnetic field lowers to $-75nT$ at the first solar contact, agreeing significantly with the magnetic field measured, while velocity fluctuation decreases to the 300-450 km/s range until 2018-11-09. As PSP progressively approaches the first aphelion, the model's radial field and velocity vary once more largely in the ranges of -50 to $10nT$ and 400 to 600 km/s. The trends in temperature and proton density comparisons are similar because the accuracy of those measures is highly dependent on the solar wind speed.

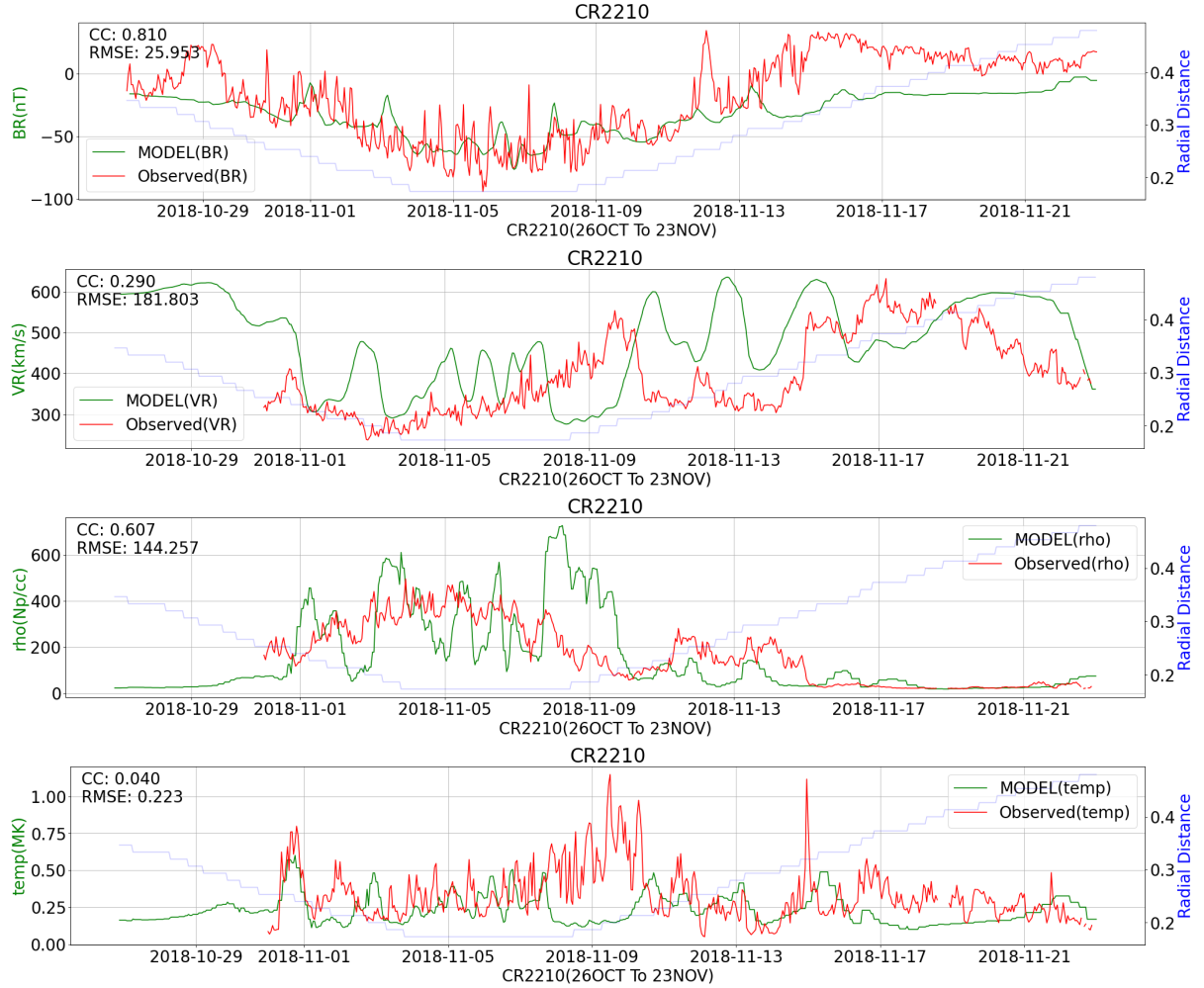


Figure 4.1: Radial components of solar wind velocity (km s⁻¹), magnetic field (nT) and proton density (cm^{-3}), temperature (MK) at PSP during the CR2210. Model results are presented in green while PSP SWEAP and FIELDS data are presented in red.

Comparison with omini data at 1 AU

For the comparison at 1 AU we again run the model and get the data. For 1 AU, model uses input data from the GONG observatory. We run the model for CR2201 which takes total 6-7 hours to generate the data. The top panel of Fig. 4.2 displays the model solar wind properties with the Omini data at 1AU .We select Omini database to get the 1AU plasma properties, which have 1 hour time resolution for the CR2210.

Figure 4.2 displays the radial components of model velocity ,magnetic field , temperature, proton density compared with Omini data for the 23 october 2018 to 23 november 2018 The model makes a fair comparison to the OMNI data, which indicate a fast wind stream of negative magnetic polarity followed by a slow wind stream of positive magnetic polarity. Nonetheless, a significant disparity exists regarding the Carrington rotation in which a coronal mass ejection (CME) impacted Earth, resulting in a potent geomagnetic storm. According to the WSA-Enlil simulation, a single coronal mass ejection occurred during the specified period. Since the launch of PSP, there have been a few CMEs traveling in Earth's direction, despite the solar wind being largely calm as the solar minimum

approaches near. It is unrealistic to expect our model to agree with OMNI data during CME crossings since the WSA model only offers information about the large-scale ambient solar wind.

We can see the model solar wind velocity data structure is quite similar to Omini data after the half CR has passed. With notable exceptions in the first 10 days of CR, in these days model overestimates the changes by as low as 250 km/s. Model's radial velocity typically agrees with small variations in the OMNI data. In the whole time of the CR , model radial magnetic field data fluctuates between -2.5 and +5nT. With regard to peak intensities and periodic polarity changes, the model's radial magnetic field compares favourably with OMNI data over the entire period, which indicate a quick wind stream of the negative magnetic polarity followed by a slow wind stream of the positive magnetic polarity. The trends in temperature proton density comparisons are similar because the accuracy of those measures is highly dependent on the solar wind speed.



Figure 4.2: Radial components of solar wind velocity (km/s),magnetic field (nT),temperature (MK) and proton density (cm^3) t Earth during the CR2210. Model results are presented in green while omini data are shown in red.

4.1.2 Using Adapt Synoptic Maps

The ADAPT model uses data assimilation, incorporating both observational data and a flux transport model to create synoptic maps. This allows ADAPT to include far-side magnetic field information and simulate the evolution of the magnetic field over time. The top panel of Fig. 4.3 displays the input field from the adapt data for CR2210. Additionally, it can be deduced from the source surface that the field exhibits roughly bipolar behaviour at $2.5 R_{\odot}$, while being quite complicated at the solar surface (see bottom panel of Fig. 4.3). The area where the magnetic field of the source surface is zero is represented by the polarity inversion line.

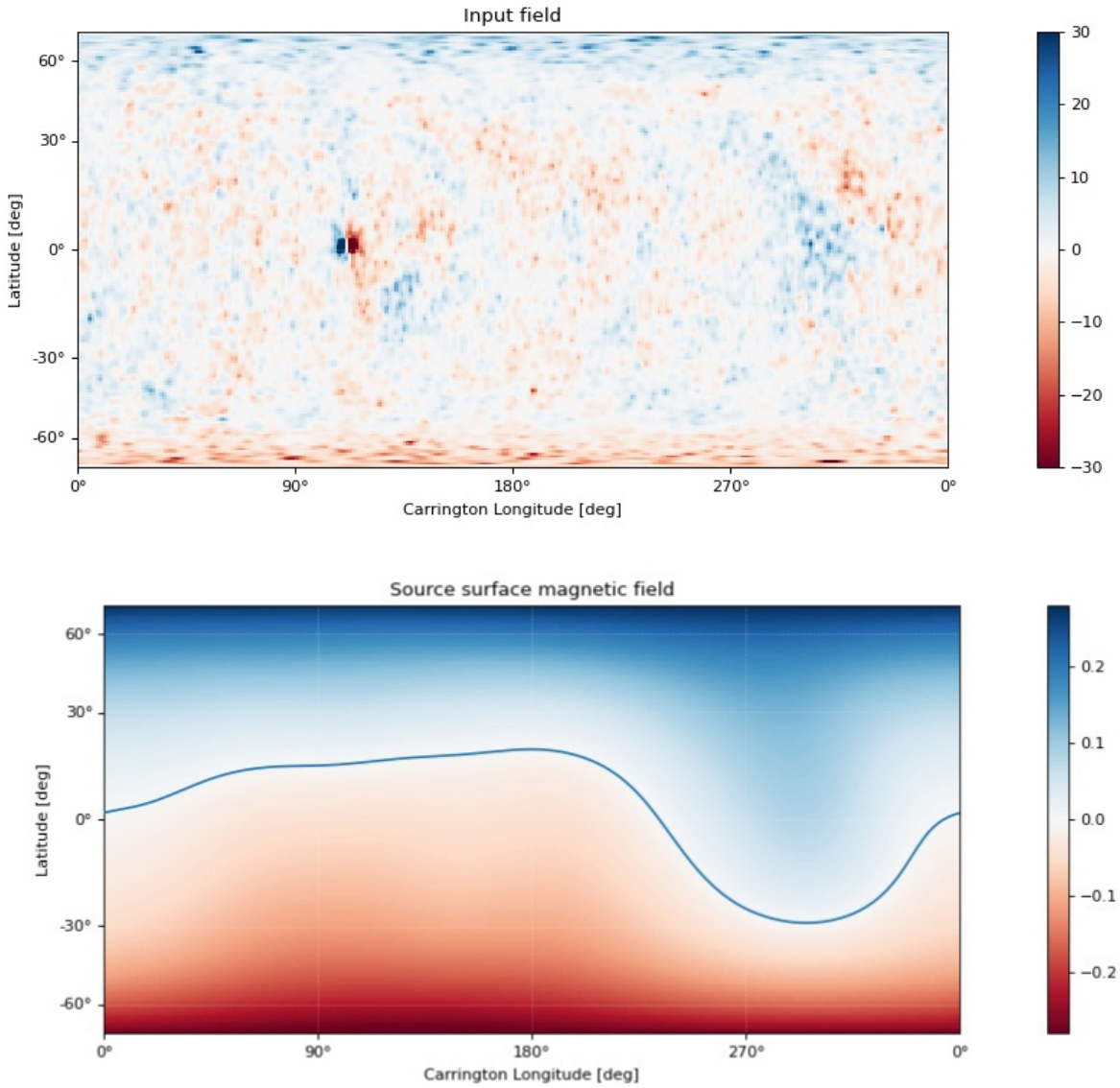


Figure 4.3: Top: Input Radial Magnetic Field for CR2210 from Adapt. Bottom: The extrapolated radial magnetic field of the source surface along with polarity inversion line shown in blue color.

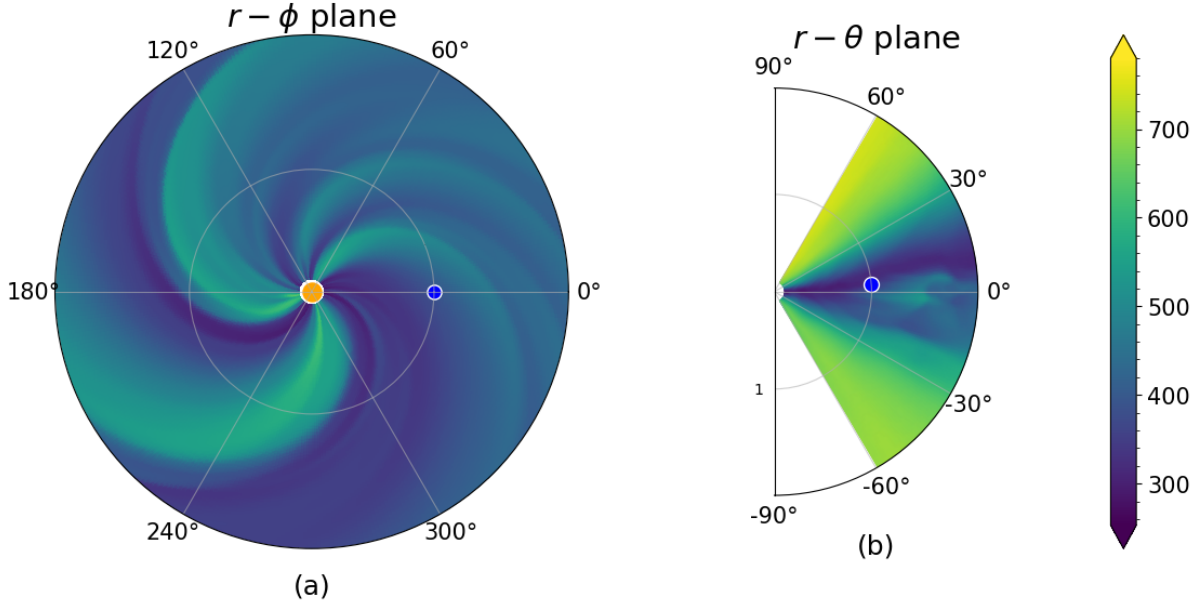


Figure 4.4: Top: The above visual displays depict the output snapshots of the inner heliospheric model CR2215 and CR2216, respectively. Panel (a) is set up in the $r - \phi$ plane at the latitude of Earth, while panel (b) is set up in the $r - \theta$ plane at a longitude of 0° .

Comparison with PSP data

The radial magnetic field and velocity at PSP of the model primarily fluctuate within the ranges of minus 50 to plus 10 nT and 300-450 km/s, respectively, as the heliocentric distance gradually decreases to 0.1 au in the starting half period of CR2210 up to 2018/11/05. This occurs when the heliocentric distance is decreasing during the starting half period of CR2210. We demonstrate that during the adapt input phase, the model generates significantly more plausible data compared to GONG. The radial magnetic field of the model decreases to -75 nT at the initial solar contact, which agrees substantially better with the magnetic field that was observed. At the same time, the variability in velocity increases to the range of 300-650 km/s till 2018-11-09, which is basically the same as PSP. As PSP moves closer and closer to its initial aphelion, the radial field and velocity of the model change significantly once more between the ranges of 50 to 10 nT and 300 to 600 kilometers per second.

When compared to the GONG input, the results that our model produces when adapt is used as an input are more exact. When we make use of adapt input, we observe that the trends improve. The GONG input provides a lot of volatility in comparison to adjust to. The trends in temperature and proton density comparisons are similar because the accuracy of those measures is highly dependent on the solar wind speed.

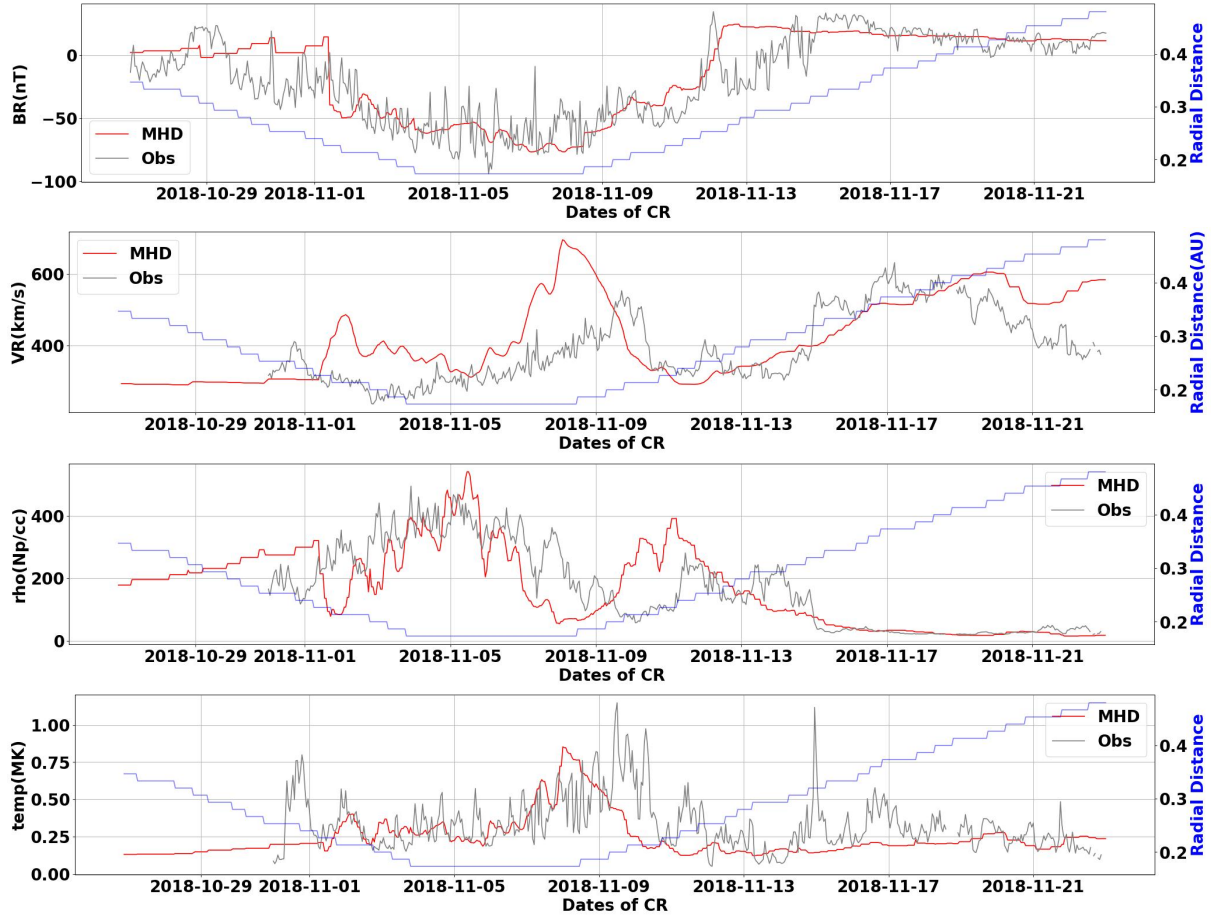


Figure 4.5: Radial components of solar wind velocity (km s⁻¹), magnetic field (nT) and proton density (cm⁻³), temperature (MK) at PSP during the CR2210. Model results are presented in red while PSP SWEAP and FIELDS data are presented in grey

Comparison with omni data at 1 AU

The comparison between the radial components of the velocity, proton density, magnetic field and temperature of the model and OMNI data for the CR 2210 during the period of October 26th, 2018 to November 23rd, 2018 around the Sun is illustrated in Figure 4.6. The model makes a fair comparison to the OMNI data, which indicate a fast wind stream of negative(-) magnetic polarity followed by a slow wind stream of positive(+) magnetic polarity.

Nonetheless, a significant disparity exists regarding the Carrington rotation in which a coronal mass ejection (CME) impacted Earth, resulting in a potent geomagnetic storm. As we discussed in previous section. It is unrealistic to expect our model to agree with OMNI data during CME crossings since the WSA model only offers information about the large-scale ambient solar wind.

The data structure of the model solar wind velocity appears to be reasonably consistent with the observed data. The radial velocity of models generally corresponds to minor fluctuations in the Omni data. The velocity profile exhibits a noticeable shift and broadening of the leftmost peak, while the remaining features of the structure demonstrate a satisfactory correspondence. Throughout the duration of the (CR) study, the radial magnetic field data of the model exhibited fluctuations ranging from negative 5 to positive 2.5 nanotesla (nT). The model's radial magnetic field exhibits a favorable

comparison with OMNI data over the entire period in terms of peak intensities and periodic polarity changes. The data indicate a rapid wind stream characterized by negative magnetic polarity, followed by a slow wind stream characterized by positive magnetic polarity. The similarity in trends between temperature and proton density comparisons can be attributed to the significant influence of solar wind speed on the precision of these measurements.

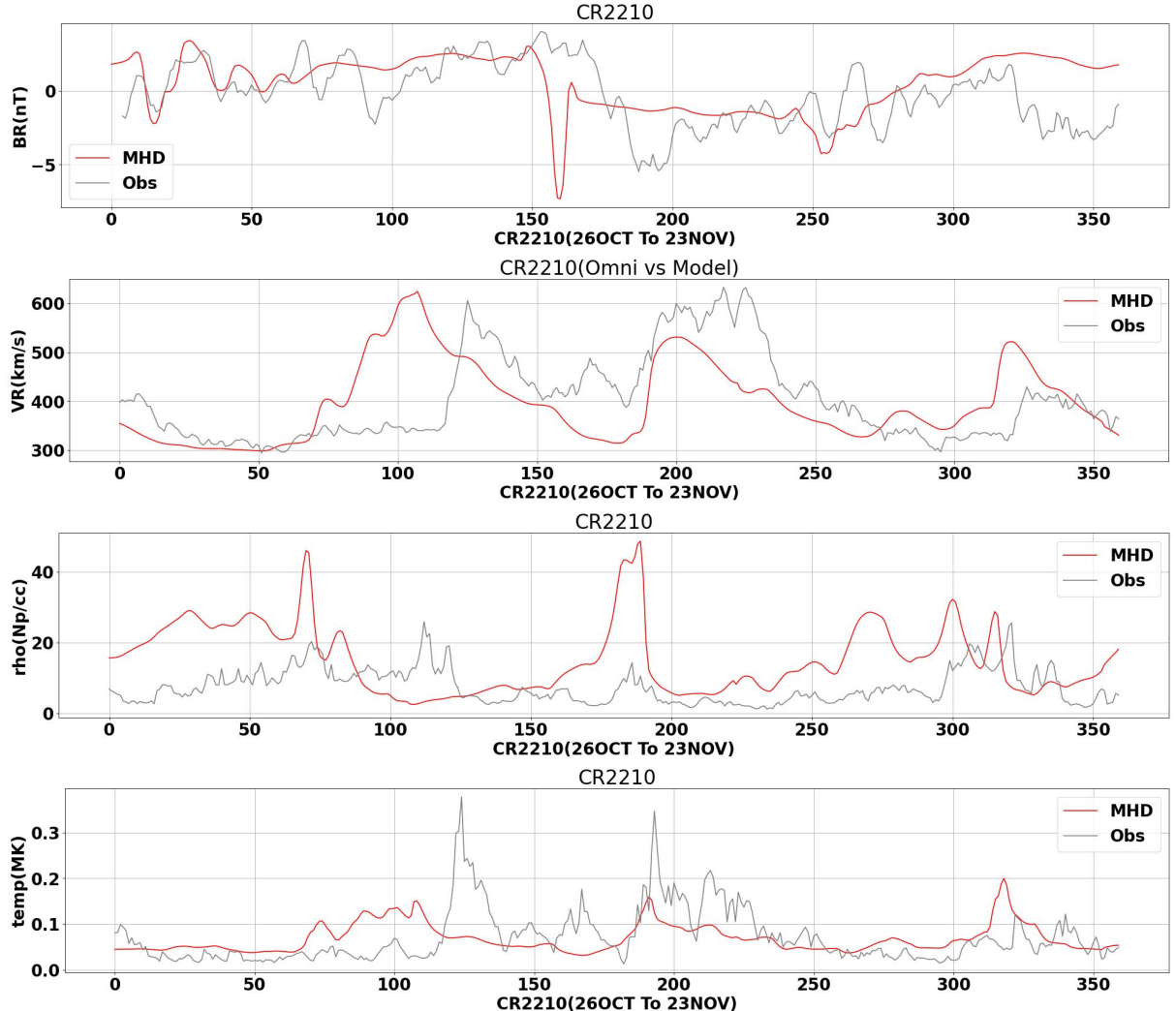


Figure 4.6: Radial components of solar wind velocity (km/s), magnetic field (nT), temperature (MK) and proton density (cm^3) t Earth during the CR2210. Model results are presented in green while omni data are shown in red.

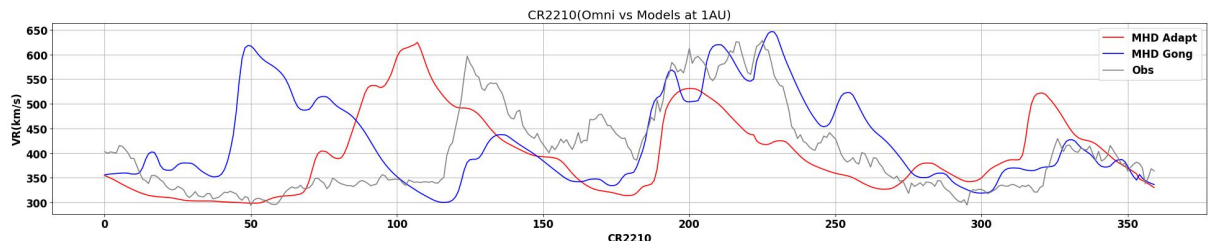


Figure 4.7: Radial components of velocity profile of model at 1AU with different inputs

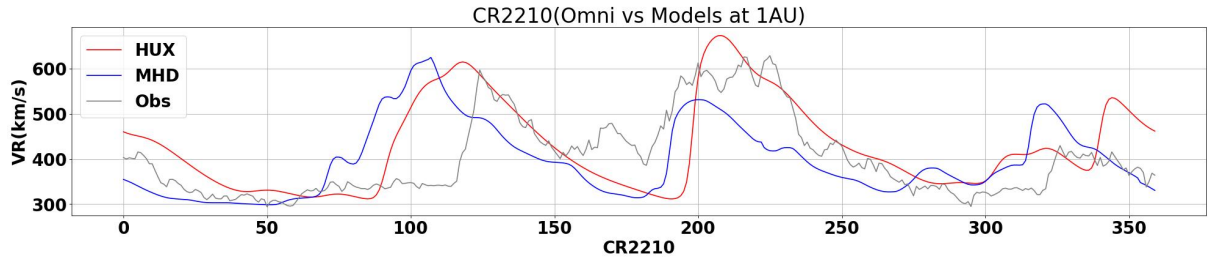


Figure 4.8: Radial components of velocity profile of HUX and MHD with observed data at 1AU (Input Adapt)

Position	Stats	SWASTI Gong	SWASTi Adapt	WSA-Enlil
L1	CC	0.36	0.52	0.44
	RMSE	108.04	85.15	110.2
PSP	CC	0.29	0.6	0.22
	RMSE	181.8	168.6	130.4

Table 4.1: Statistical Parameters of velocity profile for CR2210 with different models

Comparison with CCMC - Enlil

We also use the Community Coordinated Models Center (CCMC) to simulate the CR2210 and the conditions of the region at the PSP. We provide comparison of SWASTi model and PSP observed solar wind speed with the results generated by the Wang-Sheeley-Arge (WSA) model using the CORHEL software package available for runs-on-request basis. The CORHEL-MAS WSA ENLIL v5.0 system works by coupling the three models, providing a comprehensive and consistent representation of the solar corona and heliosphere. The system begins with photospheric magnetic field data, which are used as input for both the MAS and WSA models. The MAS model simulates the solar corona, while the WSA model computes the solar wind speed distribution near the solar surface. The output of the WSA model serves as the inner boundary condition for the ENLIL model, which then simulates the propagation of the solar wind and CMEs in the inner solar system. The final output provides forecasts of solar wind conditions at various locations, such as Earth, which can be used for space weather prediction and analysis. CORHEL is a software package that:

1. Acquires and analyzes magnetograms of the photosphere.
2. Executes the coronal model, specifically the MAS or WSA variant. The WSA was utilized in our work.
3. The outcomes are processed to produce boundary conditions for the heliospheric code.
4. The heliospheric model, specifically either the MAS or ENLIL variant, was executed (in our case, utilizing the WSA model). .

The modeling system comprises two primary components:
A semi-empirical module in close proximity to the Sun that provides an approximation

of the outflow occurring at the foundation of the solar wind. .

2. A sophisticated numerical model utilizing magnetohydrodynamics in three dimensions has been developed to simulate the evolution of resulting flows extending to the Earth.

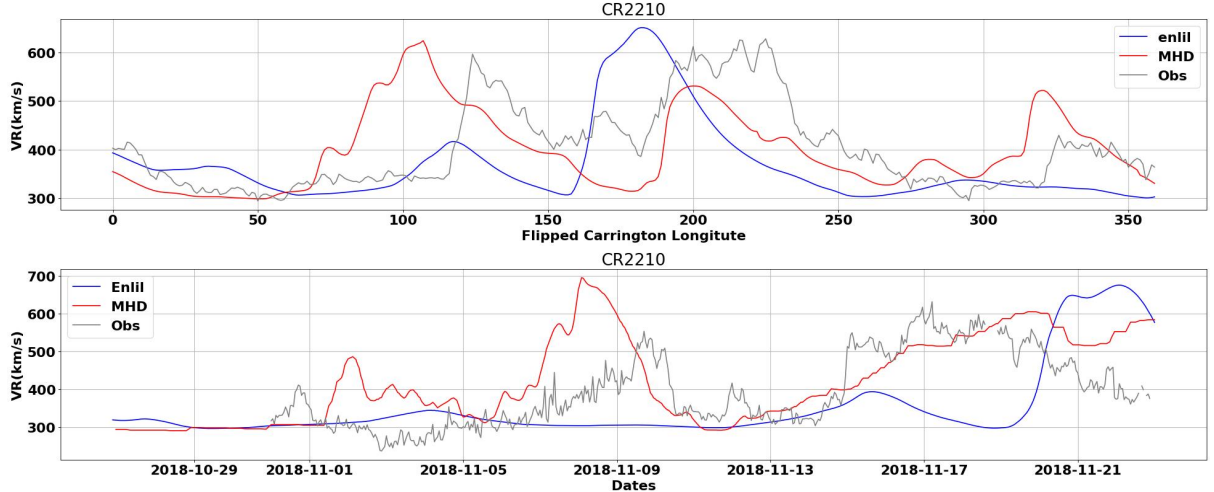


Figure 4.9: Comaprison of radial components of solar wind velocity at PSP and Earth with the Nasa’s Enlil- WSA model : Top panel comparison is at Earth and bottom panel is for PSP

CC	Enlil -WSA	SWASTi-SW
1 AU	0.44	0.36
PSP	0.22	0.60

In Figure 4.9, a comparison is presented between the WSA-Enlil and SWASTi-SW models. The top panel of the figure displays a comparison at a distance of 1AU, where it is demonstrated that the SWASTi-SW model exhibits a more accurate trend in relation to the observed data when compared to the WSA-Enlil model. The correlation coefficient for Enlil is 0.35, while the correlation coefficient for SWASTi-SW is 0.25. The comparison at PSP during CR2210 is shown in the bottom panel. While our model reasonably follows the trend here, WSA-enlil does not, as is the case with the observed data. A value of 0.21 CC is obtained for ENlil-WSA, while a value of 0.54 is obtained for SWASTi-SW.

4.1.3 Perihelion 2 of PSP (CR2215 and CR2216)

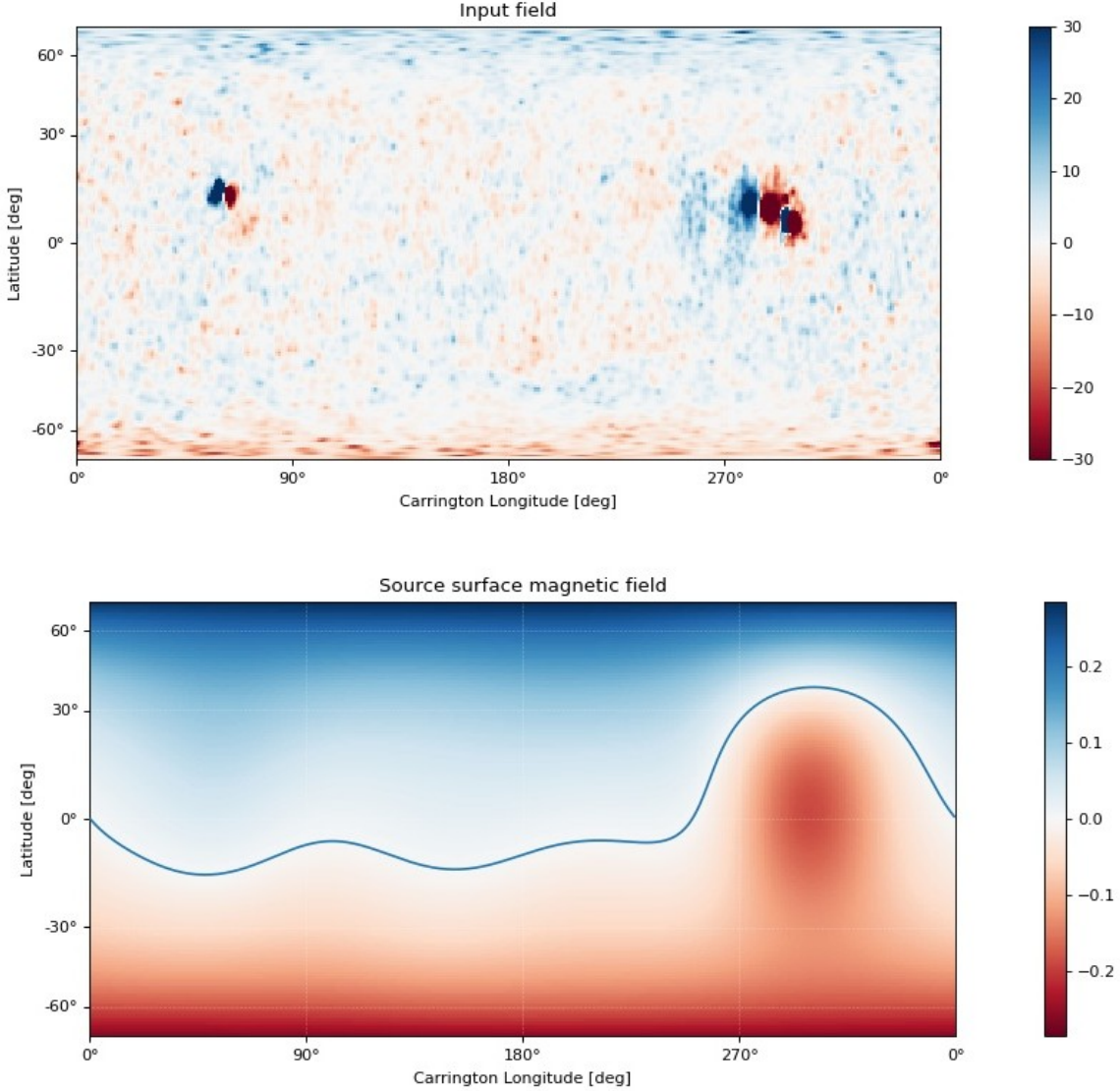


Figure 4.10: Top: Input Radial Magnetic Field(B_r) for CR2215 from Adapt. Bottom: The extrapolated radial magnetic field of the source surface along with line of polarity inversion shown in blue color.

The simulation findings at PSP for the second solar encounter over the 20-day period around perihelion 2 (2019 April) are presented in Fig. 4.12. These plots are combination of CR2215 and CR2216 because PSP second perihelion is comes under the ending of CR2215 and beginning of CR2216. According to the model, PSP undergoes a transition across the HCS (heliospheric current sheet), moving from a positive(+) to a negative(-) magnetic polarity. Subsequently, it remains situated within the negative sector following the perihelion. Conversely, as per the FIELDS data, it can be inferred that PSP was exposed to predominantly adverse magnetic polarity during the complete duration of 20 days. The PSP data indicated the presence of slow wind streams with velocities ranging from 230 to 450 km/s. However, the model's velocity exhibited fluctuations within the range of 300 to 500 km/s.

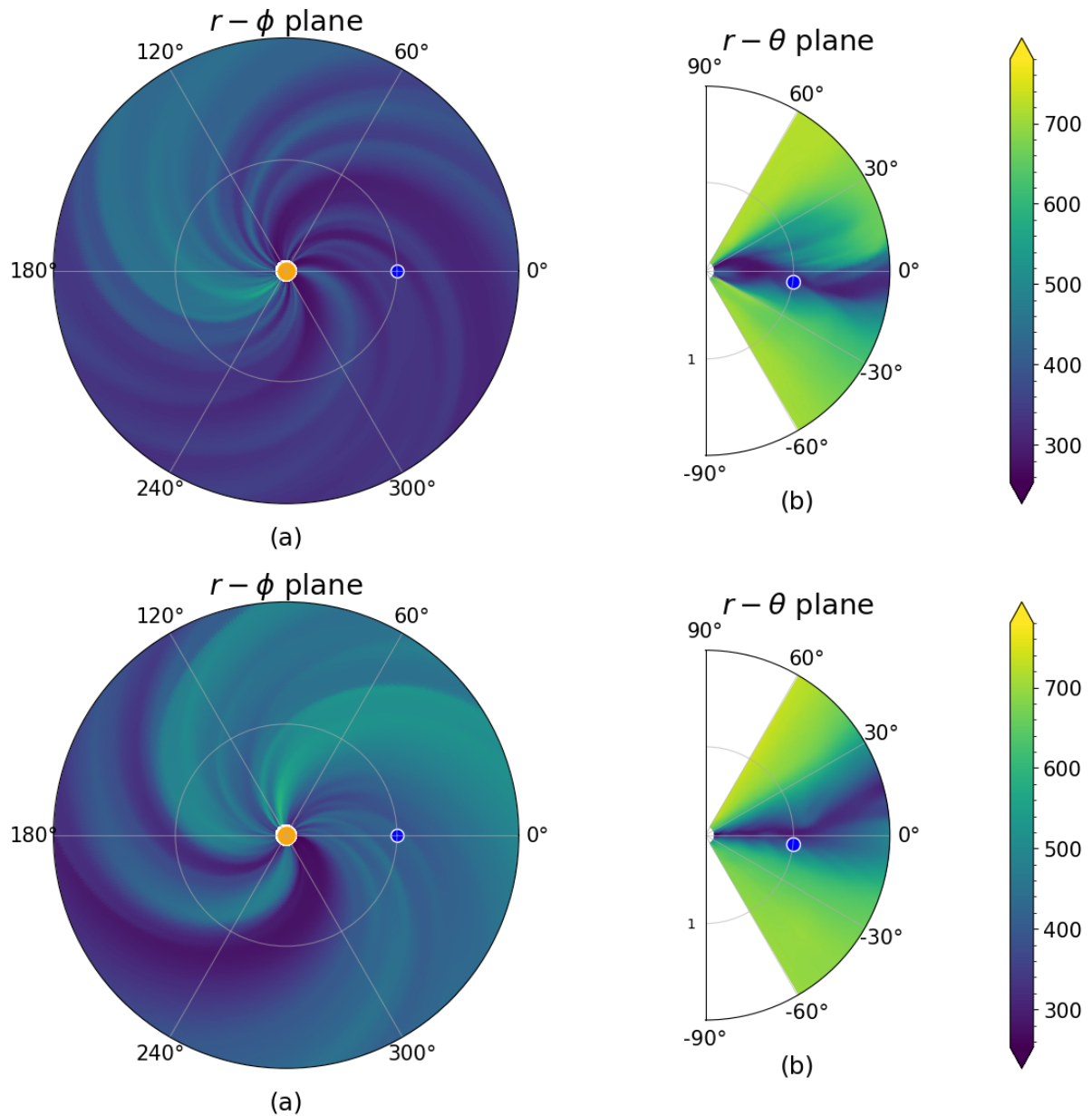


Figure 4.11: Top: The above visual displays depict the output snapshots of the inner heliospheric model CR2215 and CR2216, respectively. Panel (a) is set up in the $r - \phi$ plane at the latitude of Earth, while panel (b) is set up in the $r - \theta$ plane at a longitude of 0° .

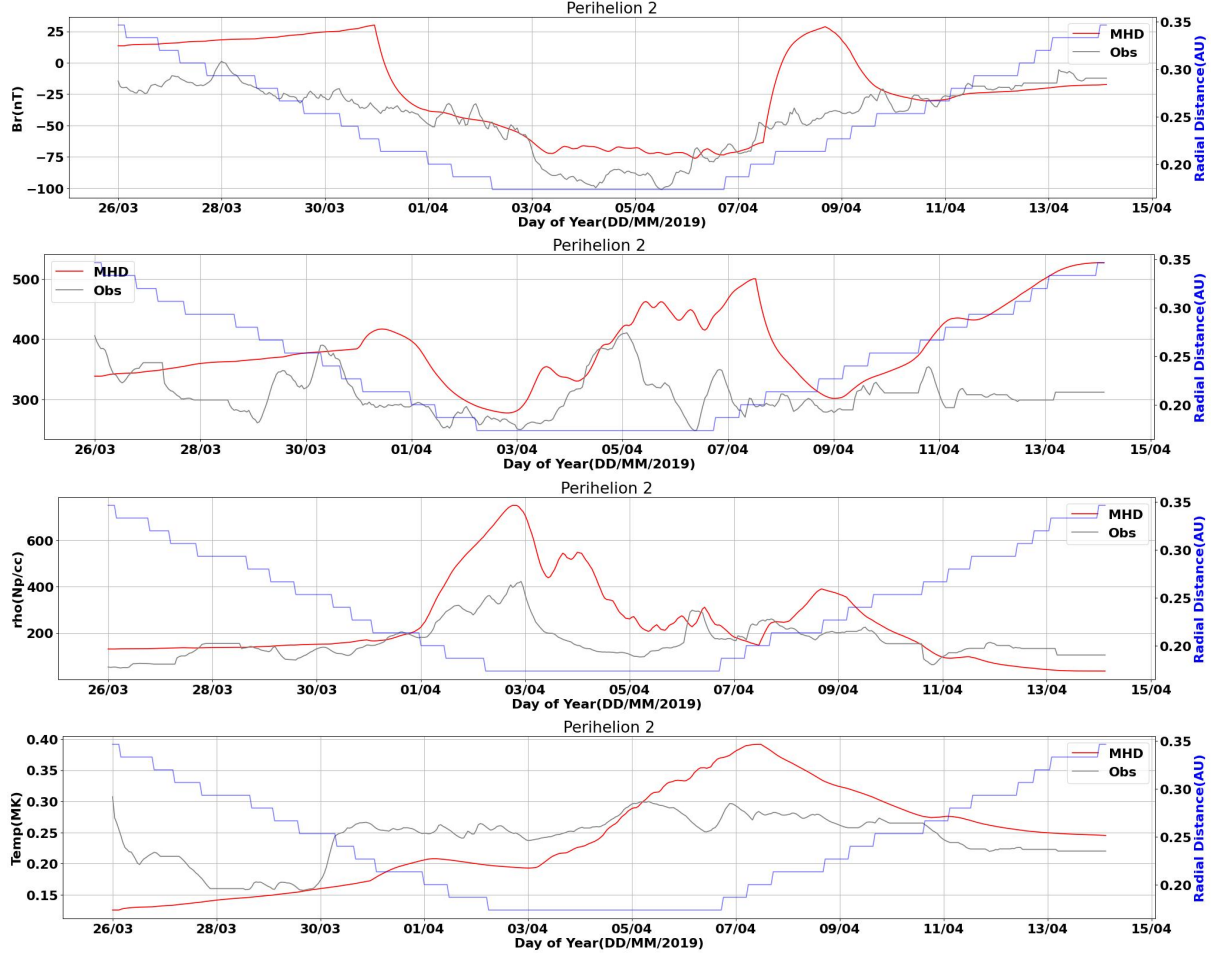


Figure 4.12: Radial components of solar wind velocity (km s⁻¹), magnetic field (nT) and proton density (cm⁻³), temperature (MK) at PSP during the second perihelion. Model results are presented in red while PSP SWEAP and FIELDS data are presented in grey

In the course of the second solar encounter, the radial magnetic field of the model experiences a rise to +25 nT, while the velocity fluctuation persists within the 400-500 km/s range until the perihelion is reached. Subsequently, the velocity fluctuation drops to the 300-450 km/s range, remaining at this level until April 9th, 2019. On Day of Year 95 (5 April), the radial magnetic field undergoes a change to -70 nT. The proton density and temperature exhibit a consistent pattern over time. The study reveals notable disparities between the model and observations during the ten-day period preceding the perihelion. Specifically, the model predicts the emergence of a high-speed stream (500 km/s) with positive magnetic polarity, which was not detected by the Parker Solar Probe (PSP).

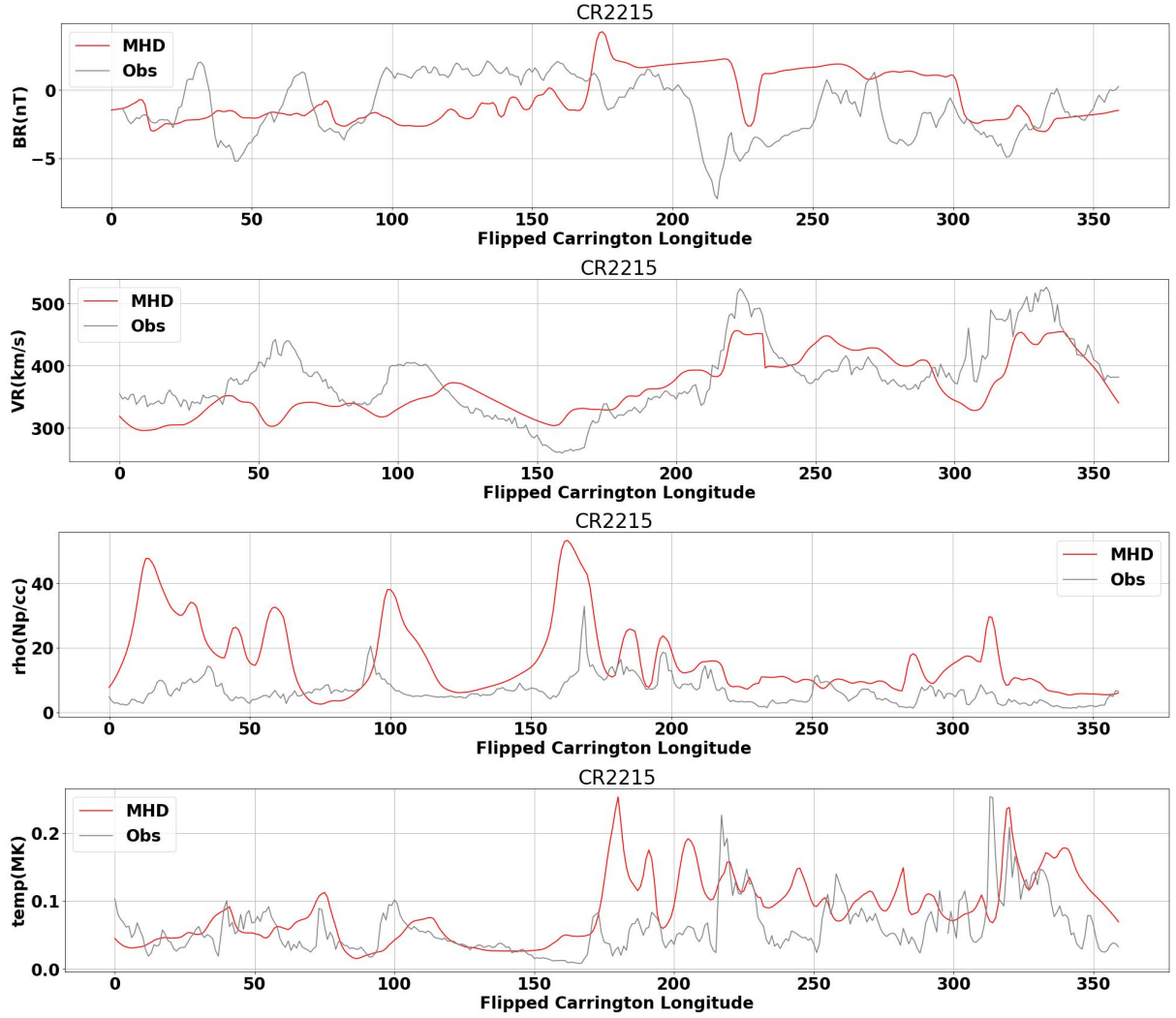


Figure 4.13: Radial components of solar wind velocity (km s^{-1}), magnetic field (nT) and proton density (cm^{-3}), temperature (MK) at Earth during CR2215. Model results are presented in red while Omni data are presented in grey

Figure 4.13 illustrates the comparison of the radial components of the magnetic field model with the velocity, proton density, and temperature data obtained from OMNI during CR2215 at Earth. The radial magnetic field of the model demonstrates peak strengths and periodic polarity changes that are comparable to those observed in the OMNI data over the entire period.

Chapter 5

Conclusion and Future Goals

A 3D time-dependent MHD simulation was conducted utilizing the SWASTi-SW model of the inner heliosphere for the initial two PSP orbits. The simulation incorporated time-varying boundary conditions acquired from the GONG and Adapt-WSA model. As delineated in the findings section, the above-mentioned boundary conditions were established to ensure optimal (most logical) concurrence between the model and proximal solar wind observations at 1 astronomical unit and at the Parker Solar Probe.

(1)The SWASTi-SW framework employed the GONG and Adapt models to corroborate the results with empirical data. The degree of accuracy in model prediction is directly influenced by the precision of the magnetogram, which serves as the sole observational input. The Adapt input model is superior in terms of data quality due to its incorporation of far-side magnetic field information and ability to simulate the magnetic field's temporal evolution.

(2)The SWASTi-SW model data is appropriately correlated with PSP data from adapt input, as evidenced by the Pearson's coefficient (CC) and RMSE value of velocity from adapt input model being superior than gong input model.

(3)When signal-to-noise ratios are enough, the SWASTi-SW model output at the first PSP perihelion during CR2210 compares reasonably with FIELDS data. A coronal hole of southern equatorial was magnetically related to PSP, according to the model during the first solar encounter before transitioning from the negative to positive sector of the heliospheric current sheet long after the perihelion of PSP orbit, which is consistent with observations and different other models described by ([Szabo et al., 2020](#)) ([Badman et al., 2020](#)) and ([Riley et al., 2019](#)).

During the final part of the second solar encounter, the model displays a discrepancy with the PSP data, as it manifests a high-velocity stream exceeding 500 km/s, which was not discernible by the spacecraft. Furthermore, based on the model's results, it is anticipated that PSP will cross the heliospheric current sheet within the perihelion region, resulting in a shift from a positive to a negative sector. Nevertheless, the observed direction of the magnetic field persisted in the radially inward direction and is hypothesized to be associated with the southern polar coronal hole during the 2nd encounter.

The structure of the solar wind has the potential to undergo unplanned modifications, even in the present era of reduced activity of Sun in the vicinity of the solar minimum. Hence, we shall revise these preliminary forecasts with more recent boundary conditions at a later stage. Several potential enhancements to the model will be taken into account prior to the subsequent prediction iterations. However, it should be noted that this outcome may not necessarily be optimal for comparison at PSP, especially during the solar encounters when the spacecraft was predominantly oriented towards the far side of the Sun. Therefore, it is imperative to consider PSP data when choosing optimal input magnetograms for future research. In this study, the PFSS model's source surface height, a free parameter, was set to 2.5 Rs. However, ([Arden et al., 2013](#)) proposed that adjusting this parameter could enhance the open flux and other related quantities at 1 au. In the subsequent investigation, we shall examine the progression of turbulence in solar wind throughout the PSP trajectory.

Chapter 6

Data Availability

The data used in this study of PSP taken from NASA SPDF (<https://spdf.gsfc.nasa.gov/>), COHOweb ([https:// spdf.gsfc.nasa.gov/](https://spdf.gsfc.nasa.gov/)), the Science Operation Centers of the four science investigation teams, and the APL Parker Solar Probe Gateway.

The utilised GONG and Adapt synoptic magnetogram maps are publicly available at https://gong.nso.edu/data/magmap_crmap.html and <http://jsoc.stanford.edu/HMI/Magnetograms.html>, respectively. The Goddard Space Flight Center, which may be reached at <https://spdf.gsfc.nasa.gov/pub/data/omni/>, provided the OMNI data. . Available at <https://pfsspy.readthedocs.io/en/stable/> is the PFSSPY Python package used in this study for PFSS modelling. You can visit <http://plutocode.ph.unito.it/> to download the MHD simulation PLUTO code for free.

Bibliography

- W. M. Arden, A. A. Norton, and X. Sun. A “breathing” source surface for cycles 23 and 24. *Journal of Geophysical Research: Space Physics*, 118(12):7888–7896, 2013. doi: 10.1002/2013JA019464. URL <https://agupubs.onlinelibrary.wiley.com/doi/abs/10.1002/2013JA019464>.
- C. N. Arge and V. J. Pizzo. Improvement in the prediction of solar wind conditions using near-real time solar magnetic field updates. , 105(A5):10465–10480, May 2000. doi: 10.1029/1999JA000262.
- Samuel T. Badman, Stuart D. Bale, Juan C. Martínez Oliveros, Olga Panasenco, Marco Velli, David Stansby, Juan C. Buitrago-Casas, Victor Réville, John W. Bonnell, Anthony W. Case, Thierry Dudok de Wit, Keith Goetz, Peter R. Harvey, Justin C. Kasper, Kelly E. Korreck, Davin E. Larson, Roberto Livi, Robert J. MacDowall, David M. Malaspina, Marc Pulupa, Michael L. Stevens, and Phyllis L. Whittlesey. Magnetic Connectivity of the Ecliptic Plane within 0.5 au: Potential Field Source Surface Modeling of the First Parker Solar Probe Encounter. *The Astrophysical Journal Supplement Series*, 246(2):23, feb 1 2020.
- S. D. Bale, K. Goetz, P. R. Harvey, P. Turin, J. W. Bonnell, T. Dudok de Wit, R. E. Ergun, R. J. MacDowall, M. Pulupa, M. Andre, M. Bolton, J. L. Bougeret, T. A. Bowen, D. Burgess, C. A. Cattell, B. D. G. Chandran, C. C. Chaston, C. H. K. Chen, M. K. Choi, J. E. Connerney, S. Cranmer, M. Diaz-Aguado, W. Donakowski, J. F. Drake, W. M. Farrell, P. Fergeau, J. Fermin, J. Fischer, N. Fox, D. Glaser, M. Goldstein, D. Gordon, E. Hanson, S. E. Harris, L. M. Hayes, J. J. Hinze, J. V. Hollweg, T. S. Horbury, R. A. Howard, V. Hoxie, G. Jannet, M. Karlsson, J. C. Kasper, P. J. Kellogg, M. Kien, J. A. Klimchuk, V. V. Krasnoselskikh, S. Krucker, J. J. Lynch, M. Maksimovic, D. M. Malaspina, S. Marker, P. Martin, J. Martinez-Oliveros, J. McCauley, D. J. McComas, T. McDonald, N. Meyer-Vernet, M. Moncuquet, S. J. Monson, F. S. Mozer, S. D. Murphy, J. Odom, R. Oliverson, J. Olson, E. N. Parker, D. Pankow, T. Phan, E. Quataert, T. Quinn, S. W. Ruplin, C. Salem, D. Seitz, D. A. Sheppard, A. Siy, K. Stevens, D. Summers, A. Szabo, M. Timofeeva, A. Vaivads, M. Velli, A. Yehle, D. Werthimer, and J. R. Wygant. The FIELDS Instrument Suite for Solar Probe Plus. Measuring the Coronal Plasma and Magnetic Field, Plasma Waves and Turbulence, and Radio Signatures of Solar Transients. , 204(1-4):49–82, December 2016. doi: 10.1007/s11214-016-0244-5.
- C. D. Bussy-Virat and A. J. Ridley. Predictions of the solar wind speed by the probability distribution function model. *Space Weather*, 12(6):337–353, June 2014. doi: 10.1002/2014SW001051.

Justin C. Kasper, Robert Abiad, Gerry Austin, Marianne Balat-Pichelin, Stuart D. Bale, John W. Belcher, Peter Berg, Henry Bergner, Matthieu Berthomier, Jay Bookbinder, Etienne Brodu, David Caldwell, Anthony W. Case, Benjamin D. G. Chandran, Peter Cheimets, Jonathan W. Cirtain, Steven R. Cranmer, David W. Curtis, Peter Daigneau, Greg Dalton, Brahmananda Dasgupta, David DeTomaso, Millan Diaz-Aguado, Blagoje Djordjevic, Bill Donaskowski, Michael Effinger, Vladimir Florinski, Nichola Fox, Mark Freeman, Dennis Gallagher, S. Peter Gary, Tom Gauron, Richard Gates, Melvin Goldstein, Leon Golub, Dorothy A. Gordon, Reid Gurnee, Giora Guth, Jasper Halekas, Ken Hatch, Jacob Heerikuisen, George Ho, Qiang Hu, Greg Johnson, Steven P. Jordan, Kelly E. Korreck, Davin Larson, Alan J. Lazarus, Gang Li, Roberto Livi, Michael Ludlam, Milan Maksimovic, James P. McFadden, William Marchant, Bennet A. Maruca, David J. McComas, Luciana Messina, Tony Mercer, Sang Park, Andrew M. Peddie, Nikolai Pogorelov, Matthew J. Reinhart, John D. Richardson, Miles Robinson, Irene Rosen, Ruth M. Skoug, Amanda Slagle, John T. Steinberg, Michael L. Stevens, Adam Szabo, Ellen R. Taylor, Chris Tiu, Paul Turin, Marco Velli, Gary Webb, Phyllis Whittlesey, Ken Wright, S. T. Wu, and Gary Zank. Solar Wind Electrons Alphas and Protons (SWEAP) Investigation: Design of the Solar Wind and Coronal Plasma Instrument Suite for Solar Probe Plus. , 204(1-4):131–186, December 2016. doi: 10.1007/s11214-015-0206-3.

J. A. Linker, Z. Mikić, D. A. Biesecker, R. J. Forsyth, S. E. Gibson, A. J. Lazarus, A. Lecinski, P. Riley, A. Szabo, and B. J. Thompson. Magnetohydrodynamic modeling of the solar corona during Whole Sun Month. , 104(A5):9809–9830, May 1999. doi: 10.1029/1998JA900159.

Prateek Mayank, Bhargav Vaidya, and D. Chakrabarty. Swasti-SW: Space Weather Adaptive Simulation Framework for Solar Wind and Its Relevance to the Aditya-L1 Mission. *The Astrophysical Journal Supplement Series*, 262(1):23, sep 1 2022.

D. Odstrčil and V. J. Pizzo. Three-dimensional propagation of coronal mass ejections (CMEs) in a structured solar wind flow: 1. CME launched within the streamer belt. *Journal of Geophysical Research: Space Physics*, 104(A1):483–492, jan 1 1999.

M. J. Owens, P. Riley, and T. S. Horbury. Probabilistic Solar Wind and Geomagnetic Forecasting Using an Analogue Ensemble or “Similar Day” Approach. , 292(5):69, May 2017. doi: 10.1007/s11207-017-1090-7.

Jens Pomoell and S. Poedts. EUHFORIA: European heliospheric forecasting information asset. *Journal of Space Weather and Space Climate*, 8:A35, June 2018. doi: 10.1051/swsc/2018020.

Martin A. Reiss, Manuela Temmer, Astrid M. Veronig, Ljubomir Nikolic, Susanne Vennerstrom, Florian Schöngassner, and Stefan J. Hofmeister. Verification of high-speed solar wind stream forecasts using operational solar wind models. *Space Weather*, 14 (7):495–510, July 2016. doi: 10.1002/2016SW001390.

Pete Riley, Michal Ben-Nun, Jon A. Linker, M. J. Owens, and T. S. Horbury. Forecasting the properties of the solar wind using simple pattern recognition. *Space Weather*, 15 (3):526–540, March 2017. doi: 10.1002/2016SW001589.

Pete Riley, Cooper Downs, Jon A. Linker, Zoran Mikic, Roberto Lionello, and Ronald M. Caplan. Predicting the Structure of the Solar Corona and Inner Heliosphere during Parker Solar Probe 's First Perihelion Pass. *The Astrophysical Journal*, 874(2):L15, mar 28 2019.

T. Rotter, A. M. Veronig, M. Temmer, and B. Vršnak. Relation Between Coronal Hole Areas on the Sun and the Solar Wind Parameters at 1 AU. , 281(2):793–813, December 2012. doi: 10.1007/s11207-012-0101-y.

Carolus J. Schrijver, Kirsti Kauristie, Alan D. Aylward, Clezio M. Denardini, Sarah E. Gibson, Alexi Glover, Nat Gopalswamy, Manuel Grande, Mike Hapgood, Daniel Heynderickx, Norbert Jakowski, Vladimir V. Kalegaev, Giovanni Lapenta, Jon A. Linker, Siqing Liu, Cristina H. Mandrini, Ian R. Mann, Tsutomu Nagatsuma, Dibyendu Nandy, Takahiro Obara, T. Paul O'Brien, Terrance Onsager, Hermann J. Opgenoorth, Michael Terkildsen, Cesar E. Valladares, and Nicole Vilmer. Understanding space weather to shield society: A global road map for 2015–2025 commissioned by COSPAR and ILWS. *Advances in Space Research*, 55(12):2745–2807, 6 2015.

Adam Szabo, Davin Larson, Phyllis Whittlesey, Michael L. Stevens, Benoit Lavraud, Tai Phan, Samantha Wallace, Shaela I. Jones-Mecholsky, Charles N. Arge, Samuel T. Badman, Dusan Odstrcil, Nikolai Pogorelov, Tae Kim, Pete Riley, Carl J. Henney, Stuart D. Bale, John W. Bonnell, Antony W. Case, Thierry Dudok de Wit, Keith Goetz, Peter Harvey, Justin C. Kasper, Kelly E. Korreck, Andriy Koval, Roberto Livi, Robert J. MacDowall, David M. Malaspina, and Marc Pulupa. The Heliospheric Current Sheet in the Inner Heliosphere Observed by the Parker Solar Probe. , 246(2):47, February 2020. doi: 10.3847/1538-4365/ab5dac.

W. T. Thompson. Coordinate systems for solar image data. , 449(2):791–803, April 2006. doi: 10.1051/0004-6361:20054262.

W. T. Thompson. Coordinate systems for solar image data. *Astronomy Astrophysics*, 449(2):791–803, mar 21 2006.

GáBor Tóth, Igor V. Sokolov, Tamas I. Gombosi, David R. Chesney, C. Robert Clauer, Darren L. de Zeeuw, Kenneth C. Hansen, Kevin J. Kane, Ward B. Manchester, Robert C. Oehmke, Kenneth G. Powell, Aaron J. Ridley, Ilia I. Roussev, Quentin F. Stout, Ovsei Volberg, Richard A. Wolf, Stanislav Sazykin, Anthony Chan, Bin Yu, and József Kóta. Space Weather Modeling Framework: A new tool for the space science community. *Journal of Geophysical Research (Space Physics)*, 110(A12):A12226, December 2005. doi: 10.1029/2005JA011126.

Bojan Vršnak, Manuela Temmer, and Astrid M. Veronig. Coronal Holes and Solar Wind High-Speed Streams: I. Forecasting the Solar Wind Parameters. , 240(2):315–330, February 2007. doi: 10.1007/s11207-007-0285-8.